Motor Memory Expansion Shapes Micro-Scale Dynamics of Naturalistic Skill Learning

Fumiaki Iwane[1], William Hayward[1], I. M. Dushyanthi Karunathilake[1], Ethan R. Buch[1], and Leonardo G. Cohen[1]*

[1]Human Cortical Physiology and Neurorehabilitation Section, NINDS, NIH, USA

*To whom correspondence should be addressed

cohenl@ninds.nih.gov

This research was supported by the Intramural Research Program of the National Institutes of Health (NIH). The contributions of the NIH author(s) are considered Works of the United States Government. The findings and conclusions presented in this paper are those of the author(s) and do not necessarily reflect the views of the NIH or the U.S. Department of Health and Human Services.

Abstract

Real-world motor skills rely on the precise spatiotemporal coordination of action sequences, progressively refined through practice. The performance of naturalistic skills depends on generating such sequences by forming motor memories that, in part, develop across rest periods interspersed with practice. Yet a critical gap remains in our understanding of how learning unfolds at a micro-scale within individual practice trials, as opposed to across trials or sessions. The moment-by-moment behavioral dynamics and their neural correlates that give rise to naturalistic skill acquisition during ongoing performance are incompletely understood.

To address this gap, we conducted two experiments in which participants learnt naturalistic sequential keypress skills of different speeds. Within each practice trial, we reproducibly identified segments of high-initial-skill (HIS)—brief periods of elevated performance followed by skill drops—that persisted throughout training. The keypress content of HIS segments scaled with execution speed and systematically increased with practice, reflecting an expansion of keypress chunk content. Importantly, this expansion of chunk content continued even after overall performance plateaued, predicting skill as training progressed.

Neural analyses revealed elevated theta–gamma phase–amplitude coupling (θ/γ PAC) and beta (β)-band bursts during HIS segments. Hippocampal θ/γ PAC notably predicted HIS segment content, identifying a possible mechanism contributing to binding individual actions into dynamic sequential enlargement of motor memory representations during early learning. These findings, inconsistent with a fatigue-based explanation, unveil expansion of motor memory capacity as a crucial contributor to early performance gains during procedural learning, bridging early cognitive control and expert skill performance.

Introduction

Motor learning, from typing to musical performance, relies on the execution of temporally precise action sequences, which constitute the core elements of fine motor expertise [1 2 3-6]. During the early stages of acquiring challenging, naturalistic skills, performance improves rapidly, with gains arising predominantly across brief rest periods interleaved with practice (micro-offline intervals)[1,7-11]. Behavioral manipulations showed that retroactive interference delivered immediately after practice reduces learning rates relative to interference imposed after a delay, consistent with a time-dependent stabilization of the motor memory [12]. Micro-offline improvements are robust and reproducible, and persist even when practice bouts are shortened to as little as 5s in duration, ruling out simple recovery from performance fatigue as their primary source [8,11-14]. Instead, converging evidence across species and techniques implicates rapid neural replay during the brief rest breaks in this offline memory consolidation process. In humans, the rate of hippocampo–neocortical replay measured with MEG [7] and the density of hippocampal sharp-wave ripples (80–120 Hz)—a canonical marker of replay— measured with intracranial EEG [13 14] predict micro-offline improvements during early learning. Importantly, Griffin et al extended these correlational findings to rhesus macaques [15]. Even more importantly, the same study provided the first causal evidence for this relationship as 20-Hz AC stimulation effectively disrupted ripple-embedded replay activity in the primary motor cortex, eliminated micro-offline performance gains in subsequent rest breaks (analogous to those interspersed with practice in humans [1,7-11,13,14] , and substantially reduced the overall learning rate for the new skill [15].

In contrast, a critical gap remains in our understanding of how learning unfolds within individual practice trials, as opposed to across trials or sessions. The moment-by-moment (i.e. - micro-scale) behavioral dynamics and their neural correlates that give rise to naturalistic skill acquisition during ongoing performance are poorly characterized. This gap is particularly important because, after only brief practice, performance in naturalistic tasks typically shifts from stimulus-driven responses to *generative* sequence production:

actions are guided by an internal memory template rather than by individual external cues, in contrast to reaction time–based paradigms[16]. The rapid emergence of this internally driven mode of performance raises the hypothesis that the capacity of the underlying skill memory becomes a key factor limiting behavior. We know from longer-term training paradigms that memory capacity expands with extended practice, and one well-established mechanism for such expansion is chunking—the grouping of individual items into larger, meaningful units. In the mnemonic domain, chunking allows a long password to be retained and produced as a small set of multi-digit segments rather than as isolated digits, effectively increasing the amount of information that can be held and manipulated in memory. [17,18] Moreover, with continued training, memory capacity may further increase by enlarging the number of action items contained within each chunk (i.e., chunk content)[19]. Together, these observations from extended training motivate the prediction that chunking-related transformations already begin to operate online, within the earliest practice trials of skill learning, and should be detectable in the fine-grained temporal structure of ongoing performance.

Motor memory capacity during early learning of keypress sequences could be expressed behaviorally as within-trial segments of high initial skill (HIS), interrupted by performance drops caused by information processing constraints. In this framework, the number of keypresses executed within a HIS segment (HIS segment content) could provide an estimate of the effective memory capacity for the practiced sequence on that trial. If this prediction is correct, one would expect HIS segments to contain more individual action elements when participants learn relatively easy skills rapidly, compared to slower, more difficult skills [20]. Moreover, with advancing training, a progressive increase in the number of action items contained within HIS segments would be indicative of an expansion of motor memory capacity[21-23]. Alternatively, micro-scale dynamics within individual practice trials could reflect reactive inhibitory factors, such as motor or cognitive fatigue [24,25]. Under this scenario, we would observe a progressive reduction in the number of action items contained within HIS segments with advancing practice, consistent with accumulating fatigue rather than an underlying expansion of motor memory capacity.

At a neural level, theta (θ, 4-8Hz)/gamma (γ, >30Hz) phase amplitude coupling (θ/γ PAC) is a mechanism supportive of memory function[26]. θ/γ PAC refers to the recurrence of identical sequences of γ bursts representing sequential memory items during specific phases of the θ rhythm[27-29]. θ/γ PAC aids in binding individual action elements into coherent sequence representations. Consistently, θ/γ ratios predict behavioral measurements of memory span[30] and correlate with memory capacity[31], although this relationship is not specific to any single memory system or task domain[32,33]. β burst oscillatory rhythms have been also linked to memory function[34-36]. Thus, higher θ/γ PAC and β burst oscillatory activity[37-39] during HIS segments could correlate with motor memory capacity.

Here, we investigated the fine-grained temporal structure of behavior and brain activity that support naturalistic skill acquisition during early ongoing performance using a series of experiments in which human participants learned a sequential keypress skill. We report that (a) periods of high initial skill (HIS) indeed emerged during individual practice trials of early learning across three different skills, (b) the content of HIS segments (number of individual keypress actions/HIS) was larger when learning fast, easier skills than slow, more difficult ones, (c) both the HIS keypress content (number of keypresses/HIS segment) and chunk content (number of keypresses/chunk) increased with practice in all three tasks, and (d) oscillatory mechanisms implicated in binding actions into memory sequences—theta–gamma phase–amplitude coupling (θ/γ PAC) and beta (β)-band bursts—were elevated during HIS segments, with hippocampal θ/γ PAC predicting HIS segment content.

Results

In **Experiment 1** (N=407), we examined the learning dynamics for naturalistic skills that varied in predicted execution speed due to differences in difficulty using an experimental paradigm described previously[16] (**Fig. S1**). Participants were randomly assigned to practice one of three 6-item sequences over 26 trials (Slow: 4-2-1-3-1-2, Skill Speed Index [SSI] =0.07, N=122; Medium: 3-1-4-2-3-4, SSI=0.41, N=127; Fast: 4-3-2-1-1-1, SSI=0.50,

N=158; where “1” is a little finger, “2” is a ring finger, “3” is a middle finger and “4” is an index finger keypress; **Fig. 1A**). Each trial comprised 10s of continuous practice followed by 10s of rest[1], and participants were instructed to perform the sequence as quickly and accurately as possible.

Segments of high initial skill (HIS) were identified in all groups

Practice elicited rapid behavioral gains across all skill groups, with larger improvements in participants training on faster sequences than on slower ones (**Fig. 1B**). As expected, fine-grained temporal performance fluctuated within practice trials, and commonly displayed a profile in which initial performance was sustained (high initial skill; HIS) for some time followed by a decline. We characterized these within-trial performance fluctuations including gains, declines and plateaus, by fitting the performance time-series from each trial with a double-sigmoid function. The end of the HIS segment was defined as the time point of maximum deceleration preceding rapid performance drops (**Fig. 1C-D**, circles; **Fig. S2A**). Consistent within-trial profiles—comprising an initial HIS segment followed by a sharp decline—emerged between trials 3 and 5 and persisted through the end of training (**Fig. S2B**). Within-subject, within-trial modeled curves were then aligned to the end of the HIS segment, revealing the robustness of this pattern across participants and skills (**Fig. 1D**). Critically, HIS segments were absent during practice of pseudo-randomized (non-repeating) sequences, even though these were executed at speeds comparable to the medium-speed skill (**Fig. S3**).

HIS segment keypress content scaled with speed of skill practice

A plausible explanation for within-trial skill drops at the end of HIS segments is motor fatigue[24,40]. In this account, each keypress incrementally increases fatigue, while recovery occurs during the intervals between keypresses, i.e., the keypress transitions times (KTT). Faster skills, with shorter KTTs, allow less time for recovery and thus produce greater cumulative fatigue. Consequently, faster skills should yield shorter HIS segments with fewer keypresses, whereas slower skills, with longer KTTs, should permit more recovery and support longer HIS segments.

We observed the opposite pattern to that expected under a fatigue account: both keypress content and duration of HIS segments increased systematically with skill speed. Mean keypress content was 10.83±0.32 (mean±sem.), 12.63±0.46 and 18.86±0.51 keypresses/HIS segment for the slow, medium and fast skills, respectively (one-way ANOVA, $F_{2,404}$=89.8, p<0.001, **Fig. 2A**), all values exceeding classic estimates of preplanning capacity[41]. Consistently, HIS segment durations were longer for faster skills (fast: 4.72±0.05 s) than for slower ones (medium: 4.18±0.07 s; slow: 4.14±0.07 s; one-way ANOVA, $F_{2,404}$=30.5, p<0.001; **Fig. S2C**). Together with the absence of HIS segments during practice of pseudo-randomized (non-repeating) sequences, the scaling of HIS segment content with skill speed argues against a fatigue-based contribution to HIS segment dynamics.

Training increased the HIS segment keypress content across skill groups

HIS segments keypress content increased as training progressed in all skill groups (linear-mixed effects models [LMM], BHFDR corrected, Slow: $F_{1,2633}$=32.0, t_{2633}=5.65, p<0.001, Medium: $F_{1,2663}$=21.9, t_{2663}=4.68, p<0.001, Fast: $F_{1,3201}$=5.90, t_{3201}=2.43, p=0.015, **Fig. 2B-C**).

Importantly, these results held when the analysis was restricted to the plateau phase of the learning curves, where virtually no further performance improvements were observed. Both HIS segment keypress content (trials 6-26, LMM, BHFDR corrected, Slow: $F_{1,2294}$=16.03, t_{2294}=4.00, p<0.001, Medium: $F_{1,2431}$=18.9, t_{2431}=4.34, p<0.001, Fast: $F_{1,3046}$=1.65, t_{3046}=1.28, p=0.198, **Fig. S4A**) and keypress rates (**Fig. S4B**) increased with practice. Thus, even after overall performance has reached a plateau, HIS segment content continues to expand with training.

Training-dependent enrichment of HIS segments is contingent upon the expansion of motor chunk content

Next, we asked whether changes in chunking organization could account for HIS segment dynamics. We used hierarchical clustering to identify chunk boundaries within HIS segments (**Fig. 2D**). For each participant, a boundary was defined wherever the duration of

a keypress transition within the sequence (KTT_{seq}) exceeded the corresponding transition duration measured outside the skill learning context (KTT_{pairs}) [42]. This procedure revealed a clear chunking structure in HIS segments across all skill groups.

The number of chunks per HIS segment was comparable across skills (slow: 7.13±0.30; medium: 7.78±0.37; fast: 7.87±0.34 chunks/HIS; one-way ANOVA, $F_{2,404}$=1.33, p=0.27; **Fig. 2E**). In contrast, chunk content (keypresses per chunk) was greater for the fast skill than for the medium or slow skills (Slow: 1.93±0.10, Medium: 1.95±0.08, and Fast: 3.84±0.26 keypresses/chunk, one-way ANOVA, $F_{2,404}$=36.5, p<0.001). Critically, chunk content increased progressively with practice in all skill groups (Slow: $F_{1,2630}$=72.1, t_{2630}=8.49, p<0.001, Medium: $F_{1,2662}$=81.5, t_{2662}=9.03, p<0.001, Fast: $F_{1,3200}$=9.03, t_{3200}=3.00, p=0.003, **Fig. 2F**) and this effect persisted when analyses were restricted to the performance plateau (trials 6–26, **Fig. S4C**). Thus, training expanded chunk content during HIS segments across skills. Taken together, these behavioral results support the interpretation that HIS dynamics during early learning reflect the expansion of a procedural memory buffer, rather than content loss driven by accumulating motor fatigue.

In **Experiment 2** (N=32), participants learned a medium-speed sequence in a magnetoencephalography (MEG) setting[1]. The goals were (i) to test the reproducibility of the behavioral effects described above and (ii) to identify physiological markers of memory expansion during HIS segments. Behaviorally, the results closely matched those from Experiment 1. Performance time courses showed the emergence of HIS segments beginning around trial 5 and persisting through the end of training (**Fig. S5A-B**). The HIS segments keypress content (14.07±0.91) increased with practice (LMM: $F_{1,985}$=9.00, t_{985}=3.0, p=0.003) while HIS segment duration remained stable ($F_{1,1020}$=1.21, t_{1020}=-1.10, p=0.27, 4.10±0.11, ≈4.0 s). Thus, training-dependent expansion of content within HIS segments was robustly replicated across two independent experiments.

Increased θ/γ PAC and β band bursting rates during HIS segments of early learning

Next, we examined θ/γ phase–amplitude coupling (PAC) [26,43,44]. Whole-brain source-space θ/γ PAC was significantly higher during HIS segments (trials 5–36) than during the

corresponding time window in pre-HIS trials (trials 1-4, paired *t*-test, t_{31}=-2.95, p=0.006, **Fig. 3A**). Parcellated source-space analyses revealed θ/γ PAC during HIS segments to be significantly elevated relative to time-shifted surrogates in contralateral hippocampus, insula, and orbitofrontal cortex, bilateral ventromedial prefrontal cortex, and ipsilateral parieto-occipital regions (cluster-forming threshold t>2.74 and distance<20mm, number of permutations=2000, p<0.01, **Fig. 3B, Table S1**). In these regions, θ/γ PAC was greater during HIS segments (0–4 s of each practice period) than during post-HIS intervals of the same trials, whether defined as 4–10 s (**Fig. 3C**) or as a duration-matched 4–8 s window (**Fig. S6A**). Critically, hippocampal θ/γ PAC strongly predicted HIS segment content (keypresses/HIS segment; LMM, $F_{1,986}$ =13.5, t_{986}=3.68, p<0.001, **Fig. 3D**) and tracked skill level across practice (LMM, $F_{1,1061}$=6.21, t_{1061}=2.49, p=0.013, **Fig. S6B**).

Examination of oscillatory bursting across frequency bands revealed selective effects in the β range. β-band burst rates were higher during HIS segments than during post-HIS segments within the same trials (whole-brain MEG sensor space; **Fig. 4A**), with no corresponding differences in other bands. β burst rates were also greater in trials containing HIS segments (trials 5–36) than in the equivalent time window of trials 1–4, before HIS segments appeared (paired t-test, t_{31}=−3.71, p<0.001; **Fig. 4B**). Source-space parcellation showed significantly elevated β burst rates during HIS segments relative to post-HIS intervals in bilateral insula and frontal, temporal, and anterior cingulate cortices (cluster-forming threshold t>3.37, distance<20 mm, 2000 permutations, p<0.01; **Fig. 4C**, **Table S2**).

DISCUSSION

We report that during procedural skill memory formation, a reproducible performance pattern of high initial skill (HIS) segments immediately followed by rapid slowing emerges within each individual in each practice trial. The number of sequential keypress actions occurring within these HIS segments (i.e. - their content) was greater for fast rather than slow learning skills. Notably, HIS segment keypress content increased progressively with

training, with more actions becoming integrated into single performance chunks, both findings inconsistent with a motor fatigue-based explanation[24]. Neural activity during HIS segments showed elevated θ/γ phase–amplitude coupling (PAC) and β-band bursts across memory-related neocortical and medial temporal regions, with hippocampal θ/γ PAC strongly predicting HIS segment content.

HIS segment content is not explained by motor fatigue

Practice led to prominent initial performance improvements followed by a phase in which average skill stabilized, limiting further gains once near-ceiling proficiency was achieved. We found that segments of HIS interrupted by skill drops emerged after the initial training trials (practice trials 3 to 5 depending on skill speed) and persisted along the plateau period in all subjects and groups. We and others have attributed these performance drops to fatigue accumulating with continued practice[1,45], particularly during the execution of fast motor tasks[45,46]. Under this scenario, each keypress results in some amount of fatigue that is recovered from during the "resting" time between keypresses (KTT)[46,47]. We reasoned that if this were the case, HIS segment content should be smaller when learning fast skills (containing more fatigue-inducing keypresses combined with shorter recovery time intervals) than for slower skills (fewer keypresses combined with longer recovery time intervals). Contrary to this prediction, we found that the keypress content of HIS segments was larger for faster skills compared to slower ones, ranging between 18 and 10 keypresses (**Fig. 2A**).

One would also expect that the accumulation of motor fatigue[24,25,46] in the course of training would result in slower typing speed and/or earlier skill drops, leading to shorter HIS segment durations with diminished keypress content. Contrary to these predictions, we observed a training-dependent expansion of HIS segment keypress content and their rates across all skills tested (**Fig. 2B-C**). These findings are inconsistent with a fatigue-based explanation of HIS content, aligning instead with reports that motor fatigue requires practice periods longer (10–60 min) than those used in this study (<9 min)[48,49]. Thus, motor

fatigue does not appear to play a pivotal role in shaping HIS segment dynamics during the early stages of mastering a naturalistic sequential skill.

HIS segment content informs on procedural memory capacity during early skill learning

Alternatively, HIS segment dynamics could inform on memory capacity during early procedural learning. We found that, depending on skill speed, HIS segments comprised between 10 and 18 keypress actions (**Fig. 2A**), vastly exceeding the 2-3 keypresses that can be preplanned in the context of skill learning[41]. Interestingly, 10-18 keypress actions also exceed the typical capacity limits of for example working memory (3-7 items)[50-52], suggesting that individual keypresses are unlikely to constitute the fundamental units of sequential skill memory as training progresses.

Next, we investigated the chunking organization of HIS segments content. As a new motor skill is learned, individual actions are grouped into "chunks", which simplify sequential execution and memory storage in situations where the number of sequence actions exceeds the constraints of memory capacity[23]. Examples of memory chunks in daily life are phone numbers or passwords, which are commonly recalled as single memory units rather than as the sum of the individual numbers or letters. We used hierarchical clustering to determine the boundaries of skill sequence chunks, each one preceded and followed by long keypress transition times (KTT)[53-55]. Within any given chunk, KTTs recorded in the context of the skill sequence (KTT_{seq}) were equal or faster than KTTs recorded in a non-sequential skill context (KTT_{pairs}, **Methods**)[53,56,57]. The key finding from this analysis was that the number of chunks per HIS segment was strikingly consistent across skill groups— around 7 (**Fig. 2E**)— close to, if not within, the range of canonical estimates of memory capacity reported in other domains, such as working memory (3-7) [50-52,58]. Thus, keypress chunks rather than individual keypresses may represent the skill memory "units" as a new skill is acquired.

Next, we examined how practice influenced the keypress content of chunks. Across all skill levels, chunk content (keypresses/chunk) expanded with training rather than

contracting (**Fig. 2F**), a pattern inconsistent with a fatigue-based account. Notably, HIS segment content continued to expand even during the plateau phase of the learning curves, despite overall performance reaching near-ceiling levels (**Fig. S4**). Interestingly, while chunk content progressively increased the overall duration of HIS segments remained relatively fixed. This suggests a relatively constrained upper bound on the temporal window over which the optimal performance state for these skills could be expressed. Altogether, these results are consistent with expansion of the procedural memory capacity during early learning [59].

Larger θ/γ PAC and β-band bursting during HIS segments

Which neural mechanisms might support the expansion of memory capacity during early learning? One candidate is theta–gamma phase–amplitude coupling (θ/γ PAC), which has been implicated in binding individual actions into coherent sequences[31,60-68] and in the active maintenance of information within other memory types (working memory) [26,43,44]. Our observation of elevated θ/γ PAC during HIS segments suggests that this coupling may facilitate the integration of individual finger representations—reflected in low frequency γ bursts[69]—into precise temporal and spatial positions within slower θ oscillations (i.e. precession), thereby encoding the identity of emerging sequences and chunks[31,60-68]. This binding mechanism, operating during motor execution, is likely reinforced during rapid consolidation periods that develop across rest intervals interspersed with practice[1]. Contributors to rapid consolidation during these rest periods of early skill learning include wakeful neural replay[7,15] and contextualization of individual sequence action representations[16].

Elevated θ/γ PAC during HIS segments was observed across a distributed network encompassing memory-related and sensorimotor integration regions (including the hippocampus, insula, orbitofrontal, prefrontal cortex, and regions within parieto-occipital and intraparietal sulci). In this context, the hippocampus emerged as a key node, as θ/γ PAC in this region strongly predicted HIS segment content (**Fig. 3D**) and actual skill (**Fig. S6B**). This observation aligns with evidence implicating hippocampo–neocortical neural

replay[1,7-11] and hippocampal ripples—established biomarkers of replay events[70]—in supporting micro-offline performance gains during early phases of naturalistic skill acquisition[13-15]. Altogether, these findings converge with the well-documented role of the hippocampus in supporting procedural memory formation[5,7,8].

Finally, we evaluated broadband neural oscillatory features associated with HIS segment content. The only frequency band differentiating transient high-power bursts during HIS versus post-HIS segments was β band, which revealed elevated burst rates during HIS segments particularly in the insula and frontal, temporal and anterior cingulate cortices. Furthermore, whole-brain β burst rates were higher in trials after HIS segments had become clearly defined (trials 5-36) than in trials preceding the emergence of HIS segments (trials 1-4). These results are in line with previous work showing that high β oscillatory activity [71], organized predominantly in bursts[38,72,73], supports procedural memory function. Thus, higher θ/γ PAC and β burst oscillatory activity during HIS segments constitute potential mechanisms supporting the expansion of memory capacity and content during early procedural learning of naturalistic sequential skills.

Limitations and future directions

In the present study we evaluated chunking of naturalistic, self-paced skill sequences using keypress timing patterns, which were generalizable across four different skill sequences and two experimental platforms (online and in-lab). It would be important for future in-lab investigations to evaluate chunking patterns of finger kinematics that evolve with learning, to determine if these patterns are consistent with the present keypress timing observations. It would also be important in the future to evaluate generalizability to other tasks, since actions dictated by presented stimuli (e.g. – reaction-time based tasks like the SRTT) likely involve additional performance-inhibiting factors than the self-paced, generative skills utilized in our study[74,75]. Another compelling avenue for future research is the relationship between procedural memory expansion and pre-[41] or online-[76] planning during initial skill learning. In the present study, we assessed neural substrates of HIS segment content for only one of the skill sequences, which was performed at a medium

speed level. Future work could expand this investigation to determine if these findings general across different skill sequences performed at lower or higher speeds, as well. Finally, we cannot exclude the possibility that performance-inhibiting factors like motor fatigue may exert a greater influence on HIS segment dynamics during longer or more effortful training protocols than those examined here.

In summary, our findings suggest that early procedural formation of a naturalistic memory may be contingent upon a gradual augmentation of procedural memory capacity, as evidenced by the content of HIS segments. Notably, this increase persists even after the overall skill speed performance reached a plateau. Elevated θ/γ PAC and β-band burst rates across memory-related neocortical and medial temporal regions, particularly hippocampal θ/γ PAC, emerged as candidate neural mechanisms supporting this expansion and skill gains.

Acknowledgments

We thank Ms. Tasneem Malik, Ms. Michele Richman, Ms. Catherine Blumhorst and NIMH MEG Core Facility staff for their support. This work utilized the computational resources of the NIH HPC Biowulf cluster (http://hpc.nih.gov). FI was partly supported by KAITOKU fellowship funded by the Japan Society for the Promotion of Science (JSPS). This research was supported by the Intramural Research Program of the National Institutes of Health (NIH). The contributions of the NIH author(s) are considered Works of the United States Government. The findings and conclusions presented in this paper are those of the author(s) and do not necessarily reflect the views of the NIH or the U.S. Department of Health and Human Services.

Author Contributions

Conceptualization: F.I., E.R.B. and L.G.C.; Methodology: F.I., E.R.B. and L.G.C.; Formal Analysis: F.I., E.R.B. and L.G.C.; Investigation: F.I., E.R.B. and L.G.C.; Writing—original draft: F.I., E.R.B. and L.G.C.; Writing—review & editing: F.I., W.H., D.K., E.R.B. and L.G.C.; Visualization: F.I., E.R.B. and L.G.C.; Supervision: E.R.B. and L.G.C.

Data and Code availability

Behavioral data collected in the first experiment will be available upon publication. De-identified data used in the second Experiment , permanently unlinked from all personal identifiable information (PII), are available (https://openneuro.org/datasets/ds006502/versions/1.0.0). The preprocessed data and analysis scripts used to generate the results in this study will be available upon publication.

Declarations of Interest

The authors declare no competing interests.

METHODS

Participants

Right-handed participants performed a well-established sequential motor learning task[77,78] consisting of repetitive typing of keypress sequences with their non-dominant, left hand. The study consisted of two experiments: The first experiment (N=407, 199 women, mean age 28.1±0.26) was performed online, while the second experiment (N=32, 16 women, mean age 26.6±0.87) was carried out at the National Institutes of Health (NIH) Clinical Center. The study was approved by the NIH Institutional Review Board (IRB). All online subjects (Experiments 1 and 2) were recruited from the Connect crowd-sourcing platform (Prime Research Solutions LLC, NY, USA) and completed a digital acknowledgement of participation before engaging in study procedures. In the first experiment, participants were excluded if they performed the task with their right hand, typed the sequence only once per practice trial, or exhibited a task inactivity period of five seconds or more in more than four practice trials (n=194). Participants for the second in-person study signed informed consent preceding testing.

Task

In the first experiment, we evaluated learning dynamics of three keypress skill sequences with different predicted speed profiles: slow, medium and fast, **Fig. S1C**). Participants completed the pseudorandomized paired keypress task described for Experiment 1 before and after the sequential motor skill learning task (**Fig. S1A**). Training comprised trials alternating between 10s of practice and 10s of rest—adhering closely to the methodological recommendations of Pan and Rickard (2015) to minimize reactive inhibition[45]. Keypress timing and finger identity were recorded on each trial, and skill was quantified as the speed of correctly executed sequences (keypresses per second)[1]. Participants, instructed to perform the sequential skill as fast and accurately as possible, were randomly assigned to practice one of the three skill sequences tested (**Fig. S1C**). Skill sequences were displayed along the practice intervals. A small dot appeared after each keypress, signaling the participants' present position within the sequence. Following

the completion of a full sequence iteration, the dot returned to the first sequence item. No feedback was provided. During rest intervals, each sequence item was replaced with an "X", and the dot disappeared. Participants were instructed to maintain fixation on the screen throughout. After the first few practice trials, behavior in this explicit motor learning task primarily consist of *generative* action sequences, in which responses were produced from an internal template rather than as *stimulus-driven* responses, as in the serial reaction time task (SRTT). A close real-world analogue is manually entering a long password into a secure online application: the sequence is retrieved from memory, while visual feedback about sequence position (typically shown as asterisks) is available but largely ignored by the user. This form of internally guided sequence production is particularly amenable to chunking, whereby groups of keypresses become bound into larger, more efficient units over the course of learning

The second experiment was carried out in-person in the NIH magnetoencephalography (MEG) lab. Subjects practiced the medium-speed sequential skill 4-1-3-2-4 over alternating 10 seconds of practice interleaved with 10 seconds of rest for 36 trials. Subjects used an MEG-compatible response pad (Cedrus LS-LINE, Cedrus Corp.) to record keypresses.

Behavioral Data Analysis

Skill Speed Index

The naturalistic SSI was derived from z-normalized keypress transition time (KTT_{pairs}) within each individual (**Fig. S1B**). Positive values corresponded to relatively fast transitions (e.g., 4–4, 3–3, 2–3), whereas negative values reflected slower transitions (e.g., 1–3, 4–2, 2–4). For each sequence, the SSI was obtained by summing the corresponding KTT scores and subsequently applying min–max normalization across all possible sequences (**Fig. S1C**). Sequences lacking all four keypress identities were excluded from further analyses.

Skill Measurement

We quantified performance by measuring the time required to complete each sequence cycle accurately and calculating the rate of correct keypresses per second (keypresses/s). To isolate learned sequence execution, we excluded the initial reaction time (from practice trial onset to the first keypress) and any transitions containing errors, encompasses prolonged transition times[79]. A keypress was considered correct if it matched any circular shift of the target sequence, ensuring that valid transitional elements were retained for skill estimation. Skill values derived from individual correct keypresses were then interpolated and extrapolated to yield a continuous, millisecond-resolution measure of skill across the entire practice interval.

Within-practice Skill Dynamics

First, we identified practice trials depicting time windows of high initial skill (HIS segments). Within-trial skill changes were calculated as the difference in correct sequence speed between the beginning and end of each practice trial, which were characterized by a regression model that includes an offset, and an exponential term:

$$L(t) = C_1 + C_2 \cdot \left(1 - e^{-\lambda t}\right) \#(1)$$

where $L(t)$ represented the group averaged within-trial skill change on practice trial, t, C_1 and C_2 controlled the initial performance and asymptote of the exponential term, and λ controlled the rate of change. Parameters $C_1 \in [0,5]$, $C_2 \in [-5,5]$, and $\lambda \in [0,2]$ were estimated using a constrained nonlinear least-squares method (*lsqcurvefit.m*, trust-region-reflective algorithm). Based on this model, we identified the onset of practice trials yielding within-trial performance declines (**Fig. 1B-D**).

Next, we identified the end of each HIS segment for trials revealing the within-trial skill drop by fitting a double-sigmoidal function $d(t)$ to the min–max normalized skill time series. This model comprised three components: a plateau skill level P, within-trial gain dynamics $G(t)$, and within-trial drop dynamics $D(t)$:

$$d(t) = P + G(t) + D(t) \#(2)$$

where,

$$P = C_0$$
$$G(t) = C_1 \cdot \left(1 - e^{-\lambda_1(t-d_1)}\right) \text{\#\#\# \#(3)}$$
$$D(t) = -C_2 \cdot \left(1 - e^{-\lambda_2(t-d_2)}\right) \text{\#\#}$$

Here, C_{0-2} controlled the magnitude of each component, λ_{1-2} the activation rate, and d_{1-2} the activation latency of the positive and negative sigmoidal functions. All parameters were constrained within the following bounds: $C_{0-2} \in [0,1]$, $\lambda_{1-2} \in [0,0.5]$, and $d_{1-2} \in [0,10000]$.

Parameter optimization was performed with 600 random initializations—300 single-sigmoid and 300 double-sigmoid fits (*lsqcurvefit.m*, trust-region-reflective algorithm). The parameter set, yielding the lowest Bayesian Information Criterion (BIC) was retained for further analysis, ensuring an optimal balance between model fit and complexity.

This modeling framework effectively isolated within-trial skill decay $D(t)$ from learning-related gains. The end of each HIS segment was defined as the time of maximal deceleration in $D(t)$ (i.e., the second derivative peak; **Fig. 1C-D** and **Fig. S2A**). We then quantified HIS segment content (keypress #, keypress rates) changes within and across-individuals.

Chunking organization

To identify chunk boundaries within learned motor sequences, we applied hierarchical clustering to individual keypress transition times (KTTs) during HIS segments[42]. Chunk boundaries were defined as transitions longer in sequential context (KTT_{seq}) than those in non-sequential context (KTT_{pairs}), reflecting natural segmentation points in performance. Within each chunk, KTTs during sequential execution (KTT_{seq}) were equal to or shorter than those observed in a non-sequential context (KTT_{pairs}), consistent with previous reports of reduced transition times within well-learned chunks[42] . To identify chunk boundaries within learned motor sequences, we applied hierarchical clustering to each keypress transition time (KTT) during HIS segments[42]. Chunk boundaries were defined as KTT_{seq} longer than

KTT_{pairs}, reflecting natural segmentation points in performance. Within each chunk, KTT_{seq} were equal to or shorter than KTT_{pairs}, consistent with previous reports of reduced transition times within well-learned chunks[53-55].

Dendrogram was created using the within-individual, absolute KTT_{pairs}-corrected KTT_{seq} values to group temporally adjacent transitions (**Fig. 2D**). The dendrogram was then cut at a threshold of zero, such that any KTT_{seq} longer than its corresponding KTT_{pair} defined a chunk boundary. We then quantified the number of chunks, average chunk content, and chunk rate within each HIS segment.

MRI acquisition

Structural MRI scanning was performed on a 3T MRI scanner (GE Excite HDxt and Siemens Skyra) with a 32-channel head coil. High-resolution, T1-weighted anatomical images (1 mm^3 isotropic MPRAGE sequence) were acquired for each participant in the in-lab experiment to perform surface-based cortical dipole estimation from MEG signals.

MEG acquisition

Continuous MEG was recorded at a sampling frequency of 600 Hz with a CTF 275 MEG system (CTF Systems, Inc., Canada) while participants were seated in an upright position. The system is composed of a whole head array of 275 radial 1st-order gradiometer / SQUID channels housed in a magnetically shielded room (Vacuumschmelze, Germany). Three of the gradiometers were malfunctioning and were not used for all recordings, resulting in 272 total MEG channels. Background noise was removed using synthetic 3rd order gradient balancing. Temporal alignment of the behavioral and MEG data was carried out using a TTL trigger signal. Head position indicator points were monitored before and after the recording in the scanner coordinate space using head localization coils placed on the nasion, left and right pre-auricular locations of the participant's head. These coil positions were also recorded in the subject's T1-MRI coordinate space using a stereotactic neuronavigation system (BrainSight, Rogue Research Inc.).

MRI data analysis

MRI data was analyzed using the FieldTrip[80], freesurfer[81] and Connectome Workbench[82]. Individual high-resolution T1 MRI was used to construct volume conduction models via single-shell head corrected-sphere approach. Source models and surface labels from the HCP-MMP atlas[82] were created for each participant using inner-skull and pial layer surfaces.

MEG data analysis

MEG data was analyzed using the FieldTrip[80], EEGLAB[83] and SpectralEvents (https://github.com/jonescompneurolab/SpectralEvents) toolboxes, and custom analysis scripts developed in MATLAB 2023b.

Preprocessing

Raw MEG data were high-pass filtered at 0.1 Hz with fourth order non-causal Butterworth filter. Powerline noise (60 Hz) and its harmonics (120 Hz) were removed by spectrum interpolation implemented in Fieldtrip. We then fitted Principal Component Analysis (PCA) using the Fieldtrip's implementation, and Independent Component Analysis (ICA) using EEGLAB's implementation of extended Infomax to the first 40 PCs. Spatial topographies and time series of all 40 ICs were visually inspected and those determined to be strongly associated with known electrocardiogram, eye movements and blinks artifacts were removed. MEG activity was then reconstructed using retained independent components and all other principal components, which were not used for ICA analysis.

Source reconstruction and parcellation

Source reconstruction of MEG data was performed using the standard pipeline in Fieldtrip. Individual volume conduction model calculated from individual high-resolution T1 MRI was used to generate the forward solution at each source dipole location. The linearly-constrained minimum-variance (LCMV) beamformer was used to compute inverse-solution from sensor-space MEG activity. The individual inverse solution data covariance matrix was obtained by averaging the mean covariance matrices of practice and rest intervals. Specifically, sensor-space MEG covariance was calculated for each 10 second

practice and rest interval and averaged over trials. The individual sample noise covariance matrix was computed from 6-mins of individual pre-training rest MEG data recorded during the same session. A total of 15,684 surface-based cortical dipoles were estimated. The individual HCP-MMP atlas model, which defines 180 parcellated cortical areas per hemisphere was used to extract source-space parcellated MEG activity by averaging activity within each cortical area.

Theta-gamma phase amplitude coupling

We measured the strength of PAC for a wide set of amplitude frequency ranges using the modulation index (MI) as introduced previously [84]. We first filtered (using pop_eegfiltnew.m from EEGLAB) continuous source-space parcellated MEG signal within the respective frequency bands of interest (θ=4-8Hz and γ=30-110Hz with a step of 5Hz and a window of ±6Hz). The frequency window of γ band was chosen such that it constituted twice the center frequency of the phase signal. This procedure ensures that the side peaks that arise if the amplitude signal is modulated by a lower-frequency phase signal are included [85]. We then extracted the instantaneous phase from the lower-frequency signal and the amplitude from the higher-frequency signal using the Hilbert transform.

During the in-lab experiment, subjects' HIS segments started at the beginning of each practice trial and finished 4.10±0.11 s later (**Fig. S5**). Thus, we extracted the time window of 0-4 s (HIS segment) and 4-10 s (post-HIS segment) relative to practice trial onset. We additionally analyzed the time window of 4-8 s to control for the time window length between HIS and post-HIS segments (**Fig. S6A**). Next, we concatenated the phase and amplitude signals for each practice trial and time window (18 phase bins) and computed the modulation index (MI) following established methods [86]. To standardize MI values across cortical areas, amplitude frequencies, and time windows, we generated 200 surrogate MIs by circularly shifting the theta-phase time series by a random interval greater than 600 samples (1s at the given sampling rate), producing a null distribution of MI values. A normal distribution was then fit to each surrogate set (*normfit.m*) to estimate its mean and standard deviation, which were used to z-transform the raw MI values. This

normalization procedure controls for potential confounds related to amplitude power, phase properties, or evoked activity due to the transition from a rest to a practice interval that might otherwise introduce spurious differences in PAC[87]. The standardized MI values therefore permit valid comparisons across time windows and amplitude frequencies[85]. Cortical parcels exhibiting significant PAC were identified as those with normalized MI values significantly greater than zero (*t*-test, cluster-based permutation correction). Finally, θ/γ PAC values within each significant cluster were averaged for subsequent analyses.

Oscillatory bursting analysis

Spectral burst analysis was conducted in both sensor and source (parcellated) space MEG data, following previously established methods[88]. Transient high-power bursts were detected and characterized using the SpectralEvents Toolbox, which identifies *spectral events* as local maxima in time–frequency power exceeding a specified threshold. The analysis was event-overlap–agnostic, with the detection threshold set at six times the median power (6×factors-of-the-median, FOM) across time for each frequency bin[71]. Bursts were detected across 1-40 Hz in a 1-Hz step from continuous MEG recordings spanning the entire task period (from the start of the first to the end of the last practice trial). Each detected event was characterized by its peak time, power, central frequency, and duration (**Fig. S7**). Event rate was defined as the number of detected bursts per second within HIS and post-HIS segments. Event duration was computed as the full-width at half-maximum (FWHM) of the power distribution in both the time and frequency domains, corresponding to the region where power exceeded half of the event's local maximum. Following the recommended procedure used in the previous studies[88] the first 1 s of each practice interval was excluded from analysis to minimize contamination from transient spectral activity associated with practice onset.

STATISTICAL ANALYSIS

We assessed the significance of several variables during the HIS segment, including the number of keypresses, keypress rate, number of chunks, chunk rate, chunk content and HIS duration. We compared these metrics across different groups and as practice progressed within each skill group. To perform the across-group comparison, we used a one-way ANOVA (*anova1.m*) followed by Tukey's honestly significant difference procedure for post-hoc analysis (*multcompare.m*). The progression of these values with practice trials was evaluated using linear-mixed effects models (LMM, *fitlme.m*). The choice of an LMM was made to accommodate inter-individual differences by including them as a random effect. All models were fitted using restricted maximum likelihood estimation. We tested the significance of fixed effects in the model using a Type III analysis of variance (ANOVA) with Satterthwaite's method (*fixedEffects.m* and *anova.m*). For behavioral evaluations, we used trial number as the dependent variable to measure trial-by-trial development of variables in HIS segments. On the other hand, within-cluster averaged θ/γ PAC was the dependent variable when predicting the number of HIS contents.

During the MEG analysis, we used a cluster-based multiple comparison correction approach to identify frequencies of interest, spatial contribution of parcellated brain regions to θ/γ PAC and β bursts[89]. This correction approach was chosen to address the multiple comparisons problem inherent in the high spatial resolution of the HCP-MMP atlas, while effectively leveraging its specific parcellation of 360 cortical brain regions.

Figures

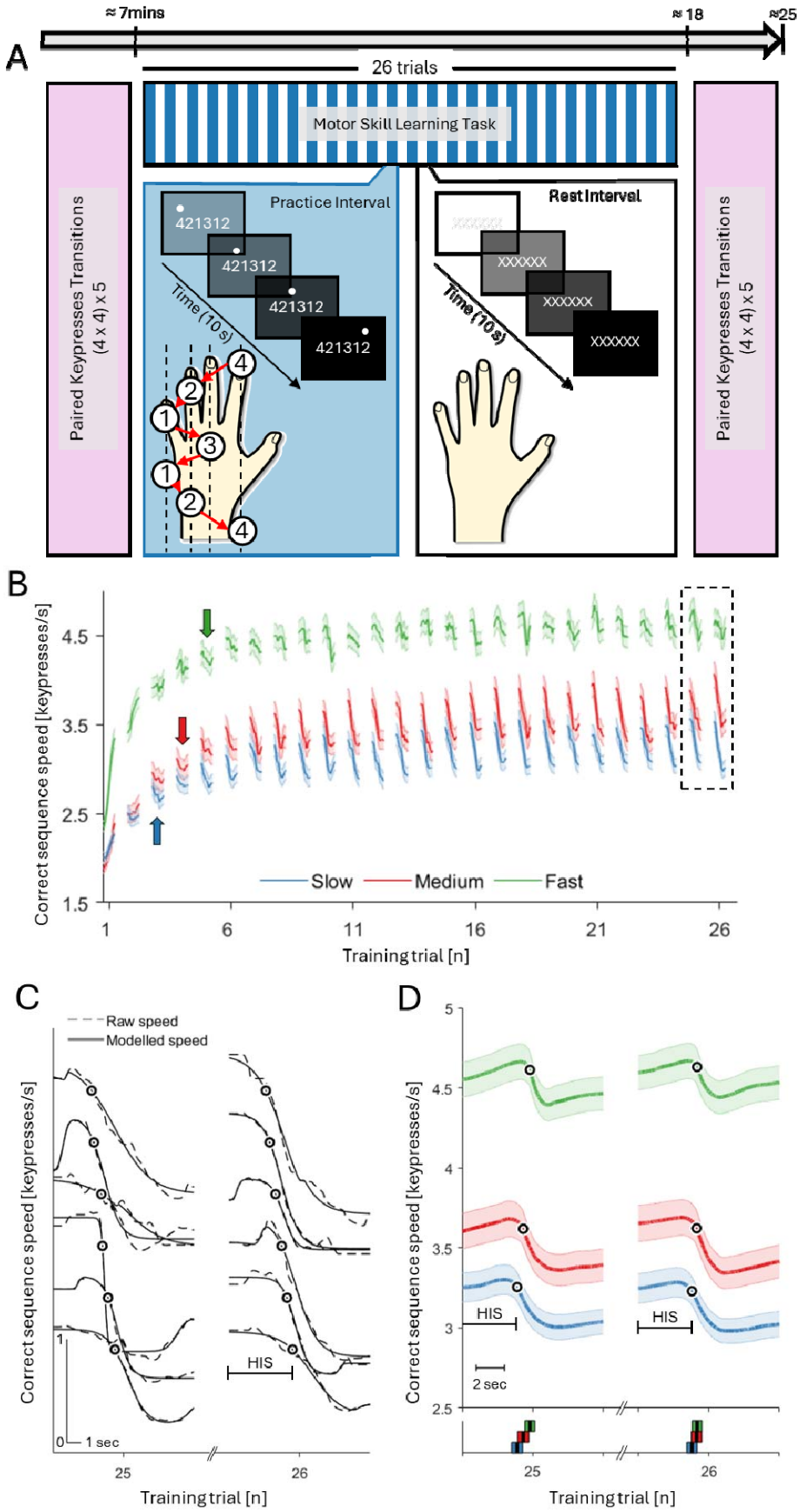
A
≈ 7mins
≈ 18
≈25
26 trials
Motor Skill Learning Task
Paired Keypresses Transitions (4 x 4) x 5
Practice Interval
421312
Time (10 s)
Rest Interval
XXXXXX
Paired Keypresses Transitions (4 x 4) x 5
B
Correct sequence speed [keypresses/s]
Training trial [n]
Slow
Medium
Fast
C
Raw speed
Modelled speed
HIS
1 sec
D
HIS
2 sec

Figure 1. Segments of high initial skill (HIS) emerged with practice across skills.

(**A**) We evaluated learning dynamics of three skill sequences of different speed: fast (SSI=0.50), medium (SSI=0.41) and slow (SSI=0.07). Participants (N=407) were randomly assigned to train one of the three skills (slow, medium, or fast) and instructed to perform the task as fast and accurately as possible following an experimental paradigm previously described[1]. Each trial consisted of 10s of practice interleaved with 10s of rest for a total of 26 trials[16]. Prior to and after training, participants also completed the pseudo-randomized paired keypress typing task described in **Fig. S1**. (**B**) Group-level performance curves (correct sequence speed [keypresses/s][7], mean±sem) in all participants. Across the three groups, rapid early gains in performance give way to a near-plateau skill level. Arrows indicate the first practice trial in which within-trial skill drops emerge, with these dynamics persisting across subsequent trials to the end of the session. (**C**) We fit a double-sigmoid function to model individual practice trial performance dynamics (**Fig. S2A**). Examples of raw (dotted lines) and modelled (solid lines) single practice trials #25 and 26 (box in **Fig. 1B**). Note the high initial skill (HIS) segments, points of maximum deceleration (circles) and following sharp performance declines. (**D**) Group level HIS segment dynamics (trials 25 and 26). Within each skill group, subjects' models were aligned to the end of the HIS segment (circle) and averaged. Mean and 95% confidence intervals of the end of the HIS segment for each group shown at the bottom.

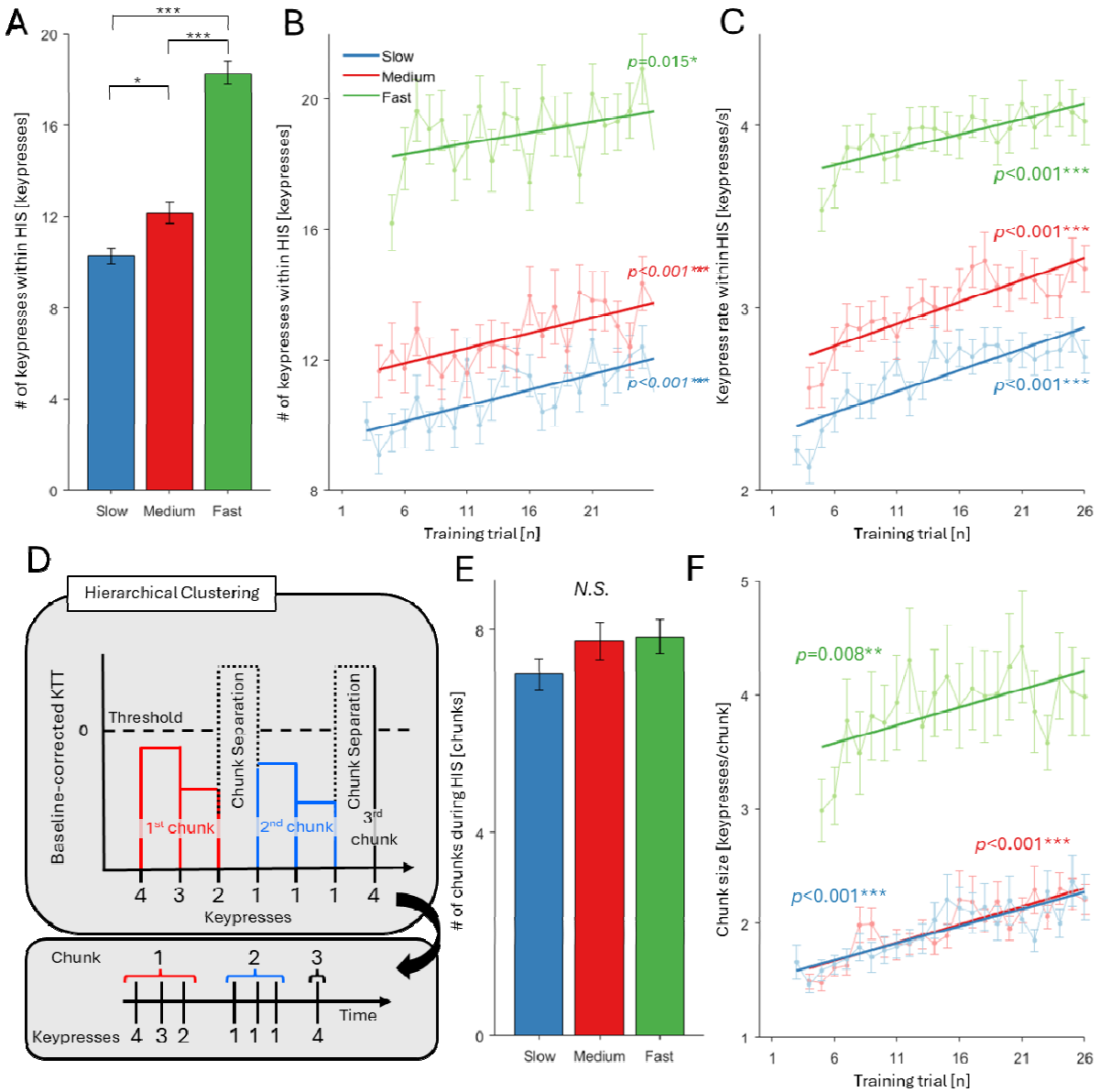

Figure 2. HIS segment keypress content increased with practice.

(**A**) HIS segment keypress content ranged between 10 and 18 keypresses and increased with skill speed. Asterisks indicate statistically significant differences during post-hoc comparisons (one-way ANOVA, $F_{2,404}$=89.8, p<0.001; *p < 0.05, **p < 0.01, ***p < 0.001). (**B**) HIS segment keypress content increased progressively with practice in all skill groups (keypresses, mean±sem; LMM, BHFDR corrected). Solid lines show the linear-fitted model for each group. Asterisks indicate statistically significant progressive increase in HIS keypress content with training. (**C**) The practice-dependent increase in HIS segment

keypress content was not simply driven by changing HIS segment durations, as keypress rates—controlling for this factor—also increased progressively with practice across all skill groups (Slow: $F_{1,2629}$=143.0, t_{2629}=12.0, p<0.001, Medium: $F_{1,2660}$=121.2, t_{2660}=11.0, p<0.001, Fast: $F_{1,3199}$=43.8, t_{3199}=6.62, p<0.001). (**D**) Hierarchical clustering was applied to within-individual, KTT_{pairs}-corrected KTT_{seq} values (KTT_{seq} – KTT_{pairs}; see **Methods**). Chunk boundaries were defined at the point where KTT_{seq} exceeded KTT_{pairs} (threshold = 0), such that longer-than- KTT_{pairs} transitions marked separations between clusters (chunks). (**E**) The mean number of chunks within HIS segments ranged between 7 and 8 for all skills. (**F**) Chunk content (keypresses/chunk) increased progressively with practice in all skill groups (keypresses/chunk, LMM, BHFDR corrected).

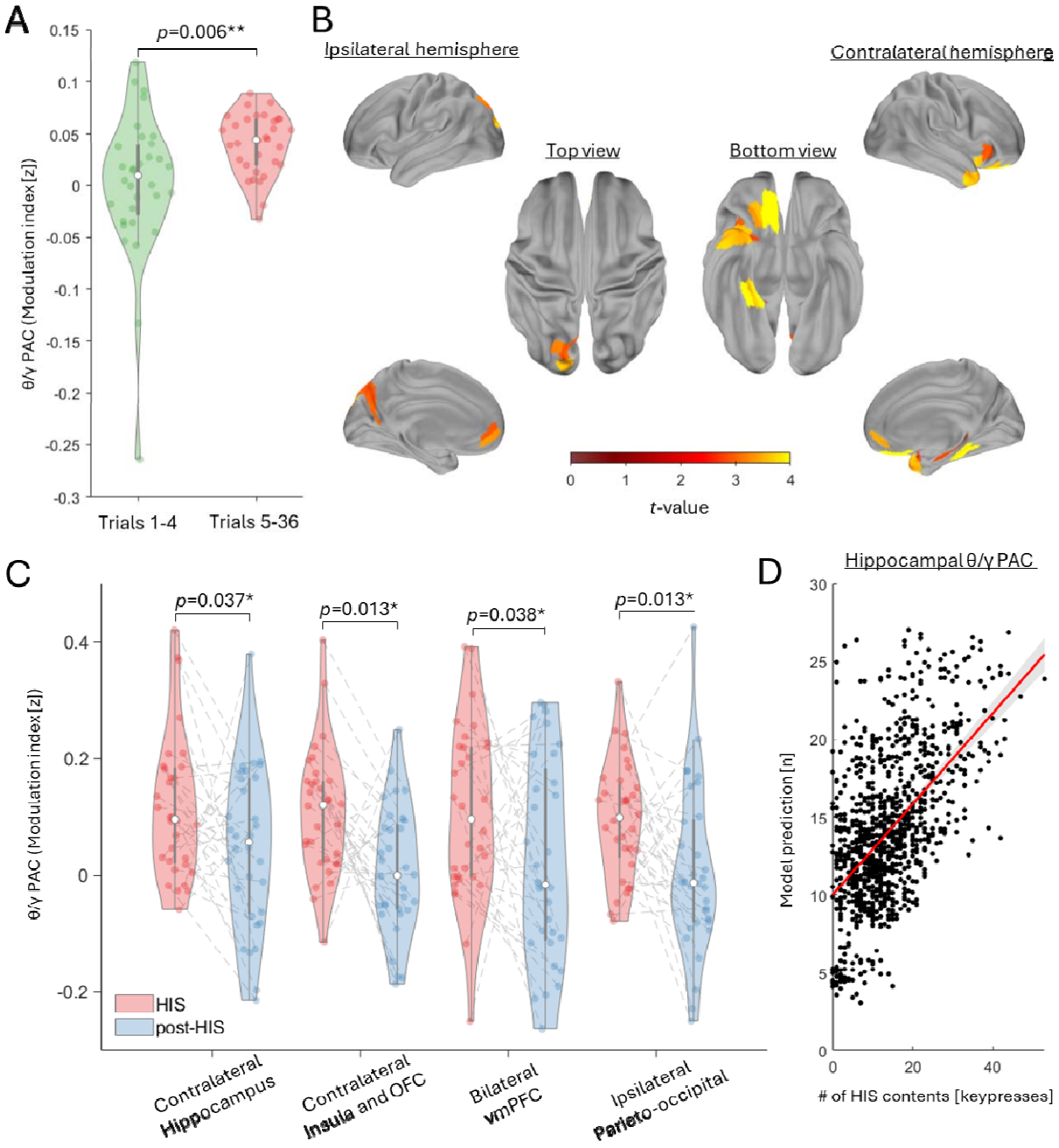

Figure 3. θ/γ PAC, HIS segment content and overall skill.

(**A**) Whole-brain source-space parcellated MEG θ/γ PAC was significantly higher during HIS segments (trials 5-36) than in the same time window of trials preceding the appearance of HIS segments (trials 1-4). Removal of two outliers did not modify the outcome (paired t-test, t_{29}=-2.56, p=0.016). (**B**) During HIS segments (trials 5-36), θ/γ PAC strength was

significantly higher in contralateral hippocampus, insula and orbitofrontal cortex (OFC), bilateral ventromedial prefrontal cortex (vmPFC), and ipsilateral parieto-occipital regions (relative to time-shifted 200 surrogates[87]; cluster-forming threshold $t>2.74$ and distance<20mm, number of permutation=2000, $p<0.01$, **Table S1**). (**C**) θ/γ PAC during HIS segments (0-4 s of each practice period) was significantly higher than following HIS segments (4-10s of each practice period) in all regions identified in **Fig. 3B** (paired *t*-test, BFDR corrected; **Fig. S6A**). (**D**) Out of these regions, only hippocampal θ/γ PAC predicted HIS segment content ($R^2=0.28$) as well as overall skill (**Fig. S6B**).

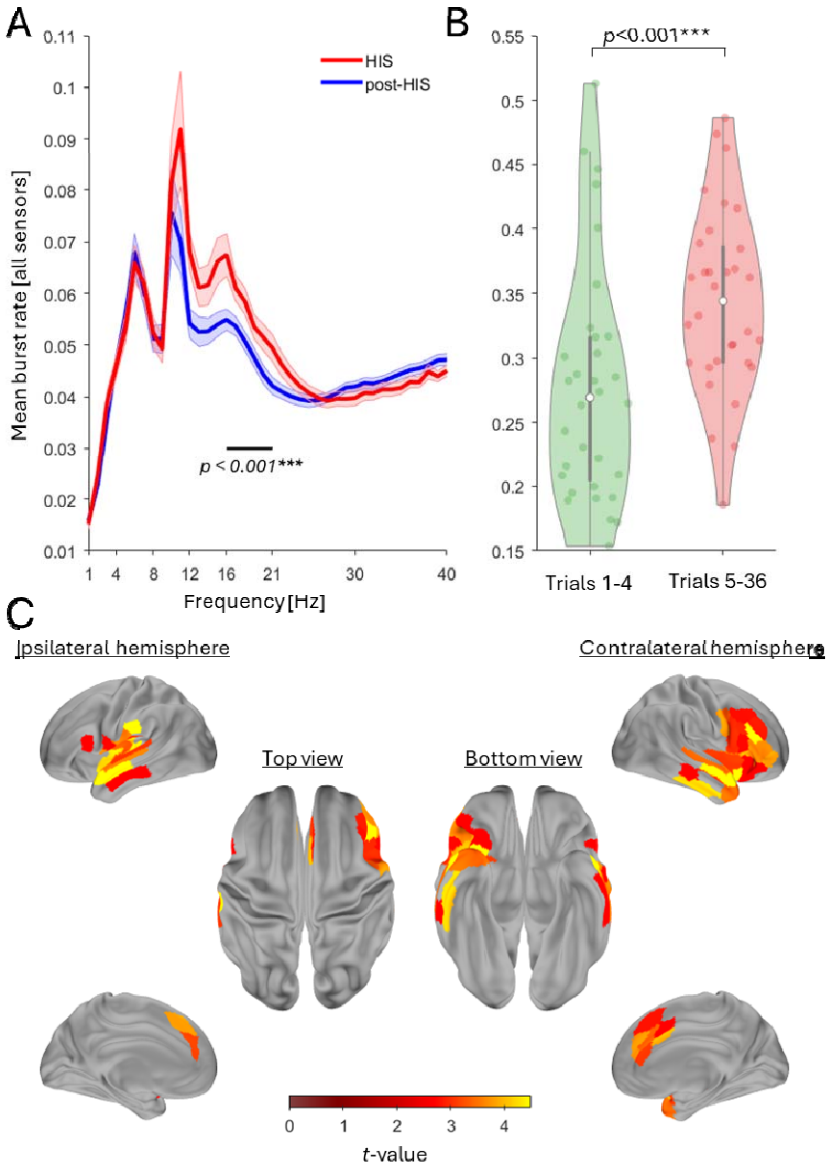

Figure 4. Beta burst activity during HIS segments.

(**A**) Broad-band whole-brain sensor-space MEG oscillatory burst rates[37] during HIS- and post-HIS segments (trial 5-36; HIS segment was determined in each trial and each participant). Note the significantly higher burst activity in the 16-21 Hz range during HIS relative to the post-HIS segments (cluster-forming threshold t>3.37, number of permutations=2000, p<0.01). β band bursts during HIS segments displayed higher power, higher frequency, and longer duration compared to bursts observed following HIS segments (**Fig S7**) (**B**) β burst rates in the 0-4 s window corresponding to the HIS segment

were significantly higher in trials containing HIS segments (trials 5–36) than in trials preceding the emergence of HIS dynamics. (**C**) Bilateral insula and frontal, temporal and anterior cingulate cortices were the main contributing regions to the higher source-space parcellated MEG β burst activity during HIS segments (**Table S2**).

Supplementary data

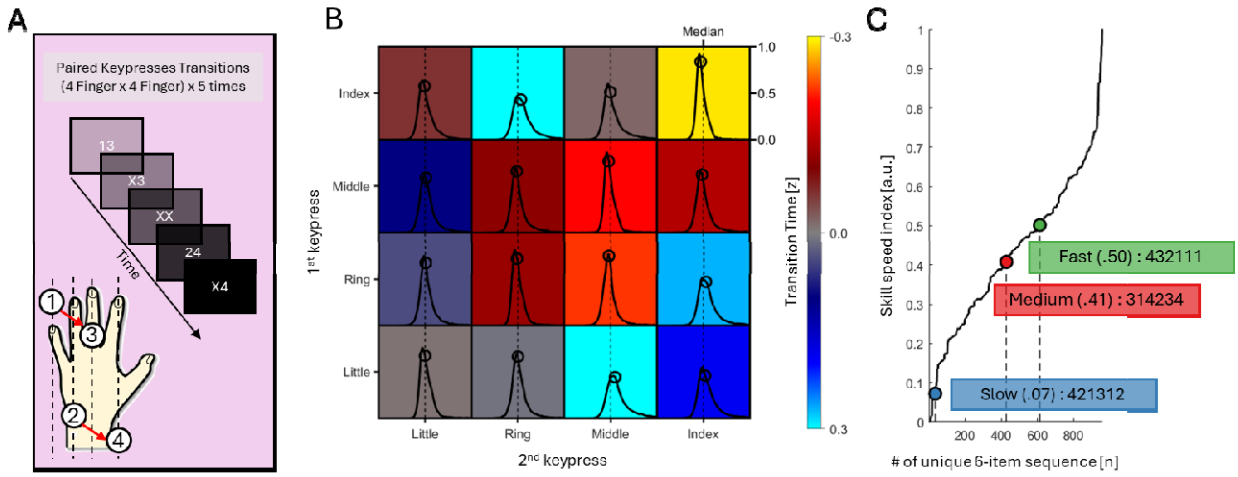

Figure S1: Naturalistic Skill Speed Index. (**A**) We first collected a large dataset of independent keypress transition times (KTTs) from healthy volunteers (N = 2,152) performing all 16 possible two-finger transitions using the little, ring, middle, and index fingers of their non-dominant (left) hand on a standard keyboard. On each trial, participants saw a pair of numeric cues (e.g., "24") indicating the required finger pair (1 = little, 2 = ring, 3 = middle, 4 = index) and were instructed to respond as quickly and accurately as possible; individual numbers were replaced with "X" as the corresponding keypresses were executed, incorrect responses triggered a repetition of the trial until correct, the inter-trial interval was uniformly jittered between 200–500 ms, and each of the 16 transitions was sampled five times in pseudorandom order. (**B**) For each participant, transition times separating keypress pairs (KTT_{pairs}) were z-normalized, and a group-level matrix of median z-score shifts for each keypress pair was constructed. (**C**) We then used this matrix to synthesize predictive estimates of the relative duration of all possible 6-item keypress sequences by summing their constituent KTT_{pairs}, thereby deriving a naturalistic Skill Speed Index (SSI) that characterizes the predicted execution speed of every possible 6-item keypress sequence. Three skills of different speed are shown.

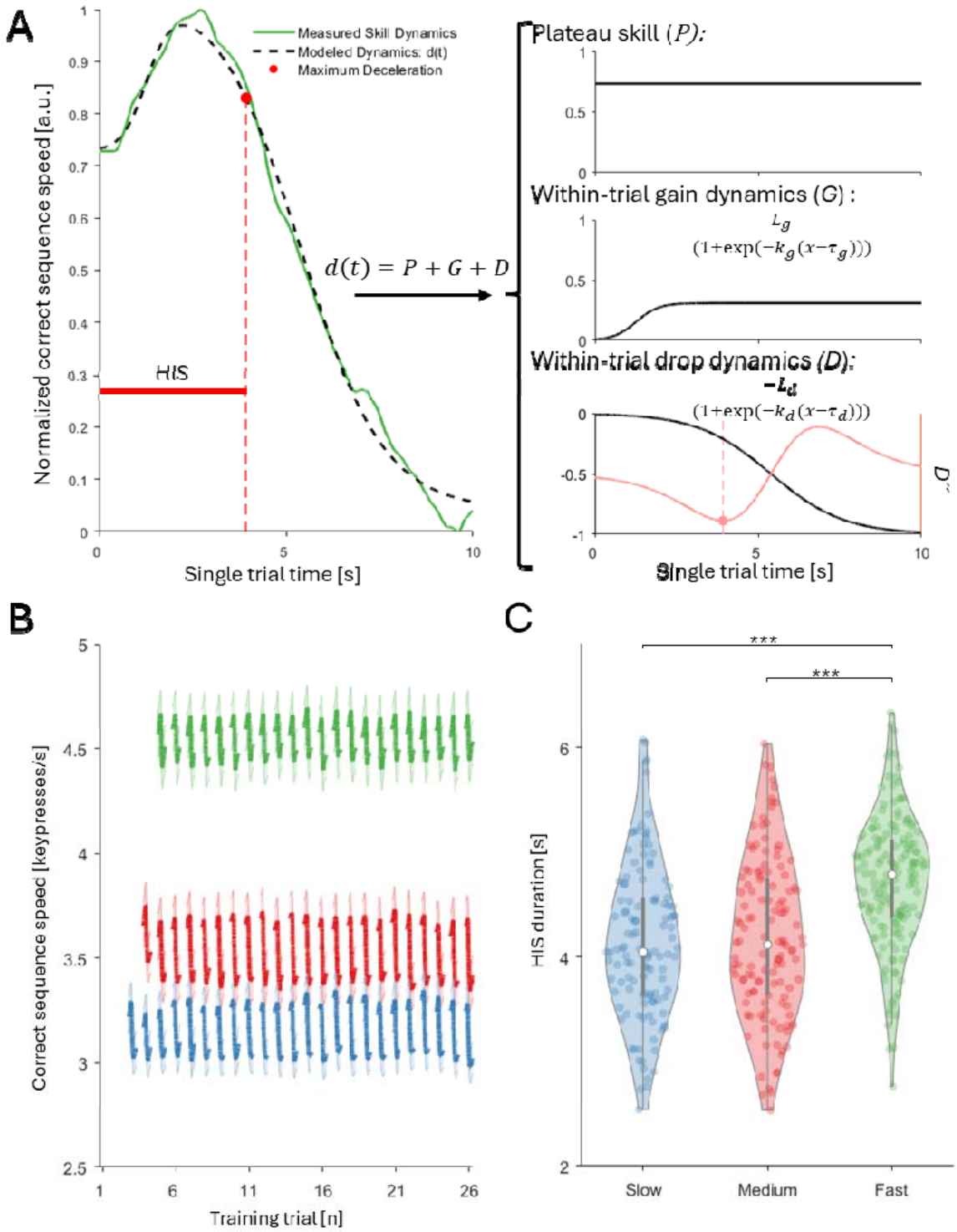

Figure S2: Modelling within-trial skill dynamics. (**A**) Skill dynamics along the full practice was modeled by fitting a double-sigmoidal function that includes plateau skill (*P*), within-

trial gain (G) and within-trial drop (*D*) dynamics. The end of the HIS segment was defined by the maximum deceleration point of the within-trial drop dynamics (2nd derivative). (**B**) Within each skill group, subjects' individual trial models were aligned to the end of the HIS segments and averaged (as shown for the last two trials in **Fig 1C-D**). Note the stability of this pattern following the emergence of HIS segments (trials 3, 4 and 5 for slow, medium and fast skills respectively). **(C)** The duration of the HIS segment was longer for the fastest skill than the slower skills. The duration of HIS segments were stable throughout the practice (Slow: $F_{1,2750}$=0.28, t_{2750}=0.53, p=0.99, Medium: $F_{1,2787}$=2.57×10^{-4}, t_{2787}=0.02, p=0.99, Fast: $F_{1,3357}$=1.75×10^{-3}, t_{3357}=0.04, p=0.99), resulting in training dependent increases in keypress rates (**Fig 2C**).

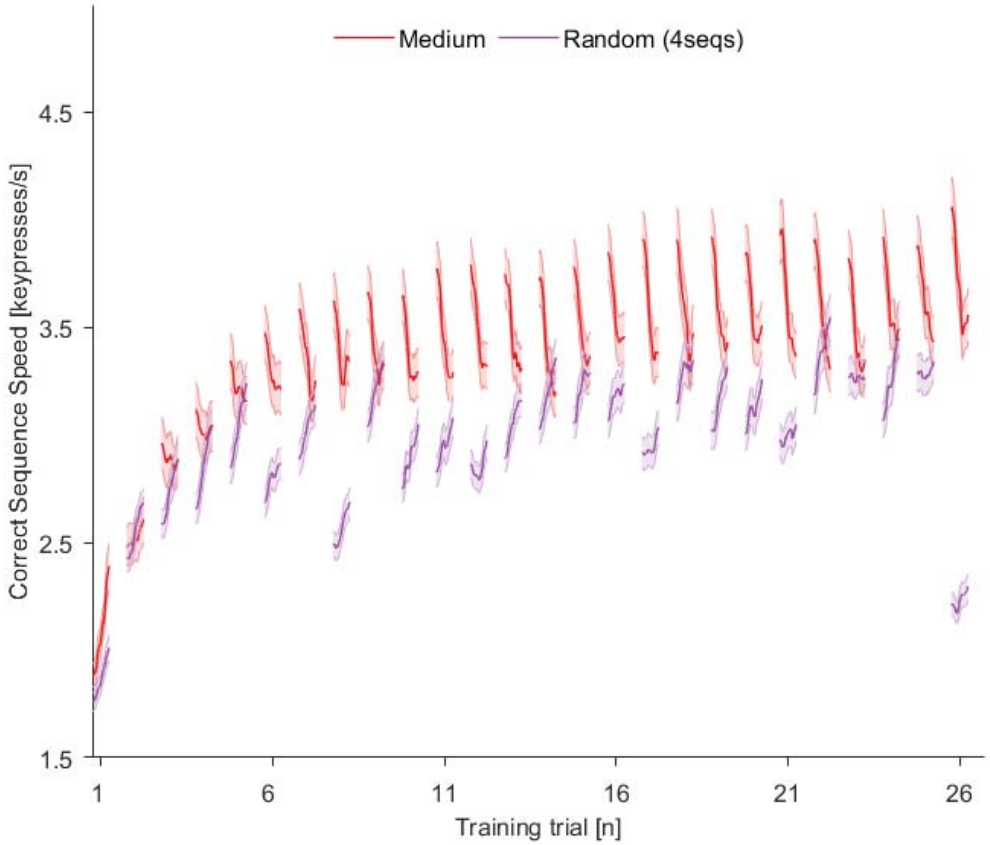

Figure S3: Practicing non-repeating sequences of comparable speed did not elicit HIS segments or substantial learning. An additional cohort (N = 156) practiced four non-repeating sequences in pseudorandom order from trials 2–25, with the same medium-speed sequence performed on trials 1 and 26. Despite comparable execution speed, intervening practice on non-repeating sequences (a) produced negligible learning of the medium sequence (first vs. last purple trials), in contrast to robust gains with repeated-sequence practice (red trials), and (b) failed to generate HIS segments. Thus, non-repetitive practice at similar speeds yielded qualitatively different within-trial dynamics, arguing against speed-related fatigue as the origin of HIS segment structure.

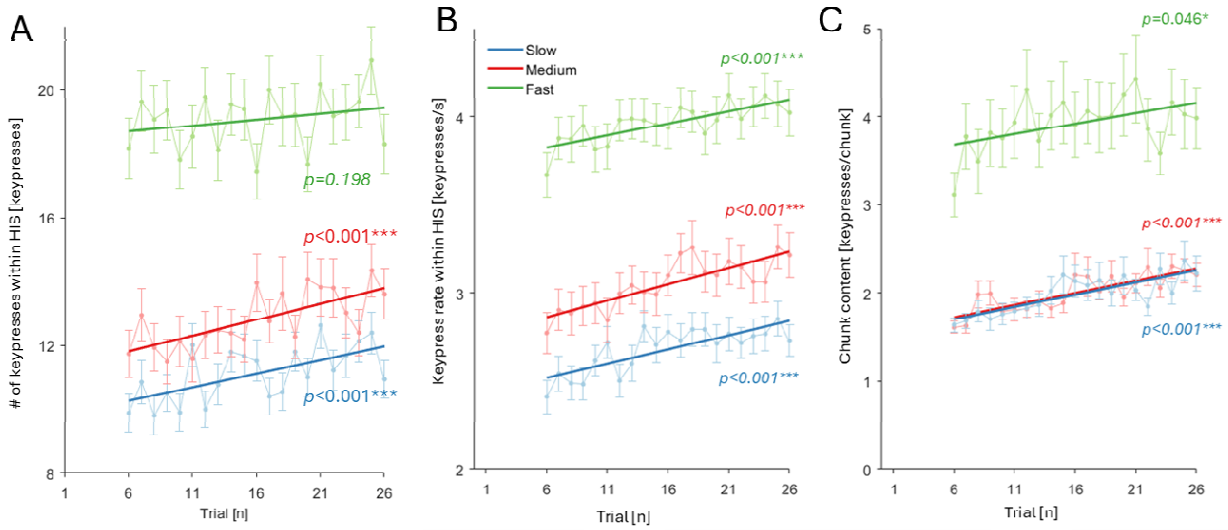

Figure S4: HIS segment content continues to expand afer skill plateaus. HIS segment content during the plateau skill period (trials 6-26) continued increasing with practice. The practice-dependent increase in HIS segment keypress content during the plateau period (**A**) was not simply driven by changing HIS segment durations, as keypress rates (**B,** LMM, BHFDR corrected, Slow: $F_{1,2291}$=45.2, t_{2291}=6.73, p<0.001, Medium: $F_{1,2430}$=58.4, t_{2430}=7.64, p<0.001, Fast: $F_{1,3044}$=24.4, t_{3044}=4.94, p<0.001)—controlling for this factor—also increased across skill groups. (**C**) Chunk keypress content increased with training in all skill groups (LMM, Slow: $F_{1,2292}$=39.2, t_{2292}=6.26, p<0.001, Medium: $F_{1,2432}$=45.7, t_{2432}=6.76, p<0.001, Fast: $F_{1,3045}$=3.98, t_{3045}=2.00, p=0.046). Thus, HIS segment content continued to expand with training even during the behavioral plateau, when overt performance gains were minimal.

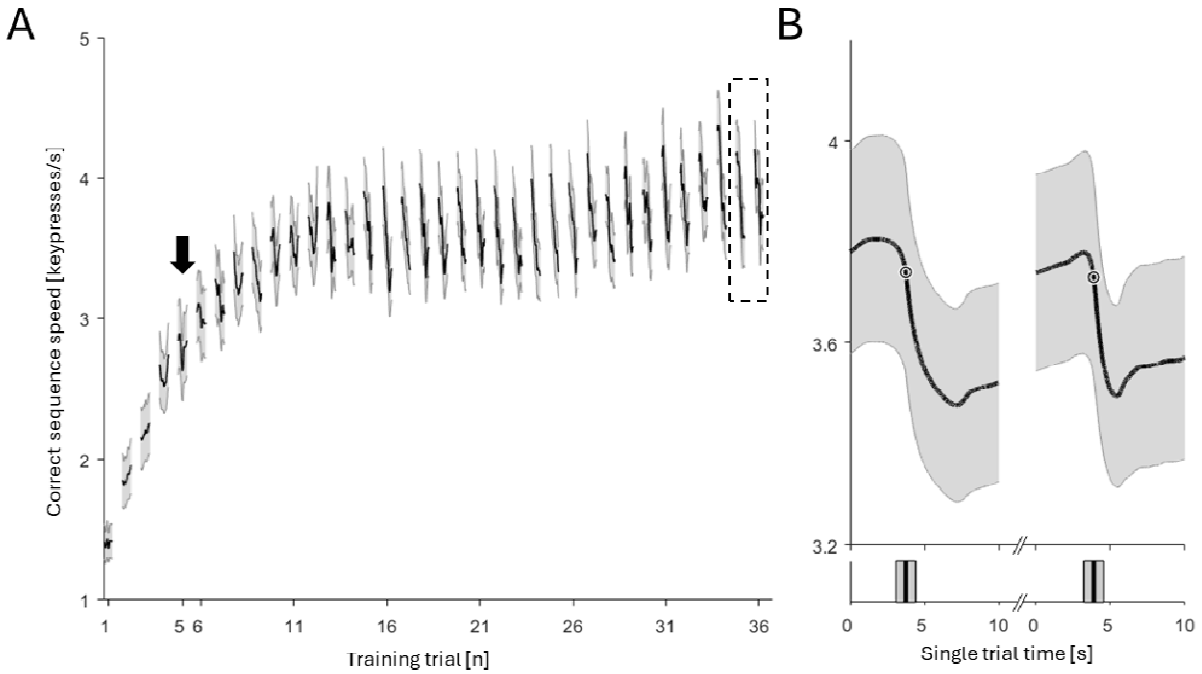

Figure S5: Replication of HIS dynamics in an independent MEG dataset. In Experiment 2, we examined MEG oscillatory dynamics in participants learning a medium-speed sequential skill over 36 practice trials (N = 32; https://openneuro.org/datasets/ds006502/versions/1.0.0). **(A)** Performance curves, computed as in Experiment 1, revealed the emergence of high-initial-skill (HIS) segment dynamics around trial 5 (arrow), closely paralleling the onset observed previously (arrows in **Fig 1B**). **(B)** Group-level intra-trial performance profiles for the last two trials (35 and 36), aligned to the end of the HIS segment and averaged as in Experiment 1, show the same characteristic within-trial pattern. Thus, the HIS segments intra-trial dynamics described in Experiment 1 were reproduced in an independent cohort and recording environment.

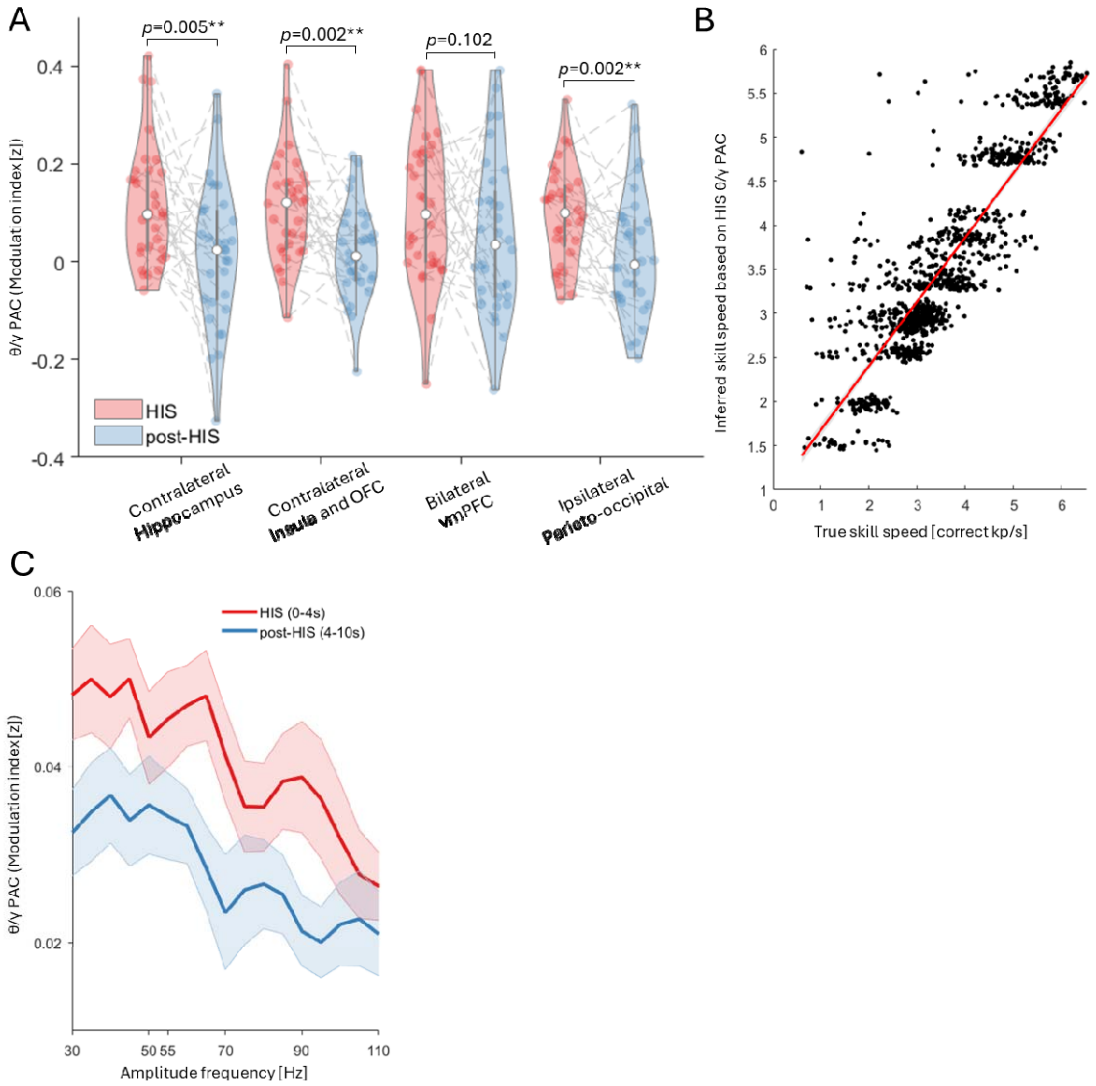

Figure S6: Complementary θ/γ PAC analyses. **(A)** We compared θ/γ PAC during HIS segments (0–4 s) with duration-matched θ/γ PAC during the immediately following interval (4–8 s). The resulting spatial pattern closely matched that obtained in **Fig 3C**, which used a slightly longer post-HIS window (4–10 s). No significant predictive effects were observed in the other regions (contralateral insula/OFC: t_{986}=1.29, p=0.39; bilateral vmPFC: t_{985}=−0.36, p=0.72; ipsilateral parieto-occipital: t_{987}=0.44, p=0.72). (**B**) Hippocampal θ/γ PAC during HIS segments was used to model skill performance (mean correct sequence speed) using linear mixed-effects models. The modeled speeds derived from hippocampal θ/γ PAC (y-axis) closely tracked the observed mean skill speeds of practice trials (x-axis), indicating that hippocampal θ/γ PAC reliably predicted skill level across practice. (**C**) Whole-brain

source-space θ/γ PAC strength, parcellated across regions and normalized by 200 time-shifted surrogates, was quantified during HIS and post-HIS segments (mean ± SEM; θ = 4–8 Hz, γ = 30–110 Hz in 5-Hz steps with ±6-Hz windows; trials 5–36). Because θ/γ PAC was strongest in the 30–55 Hz range, this γ-band interval was used for all analyses.

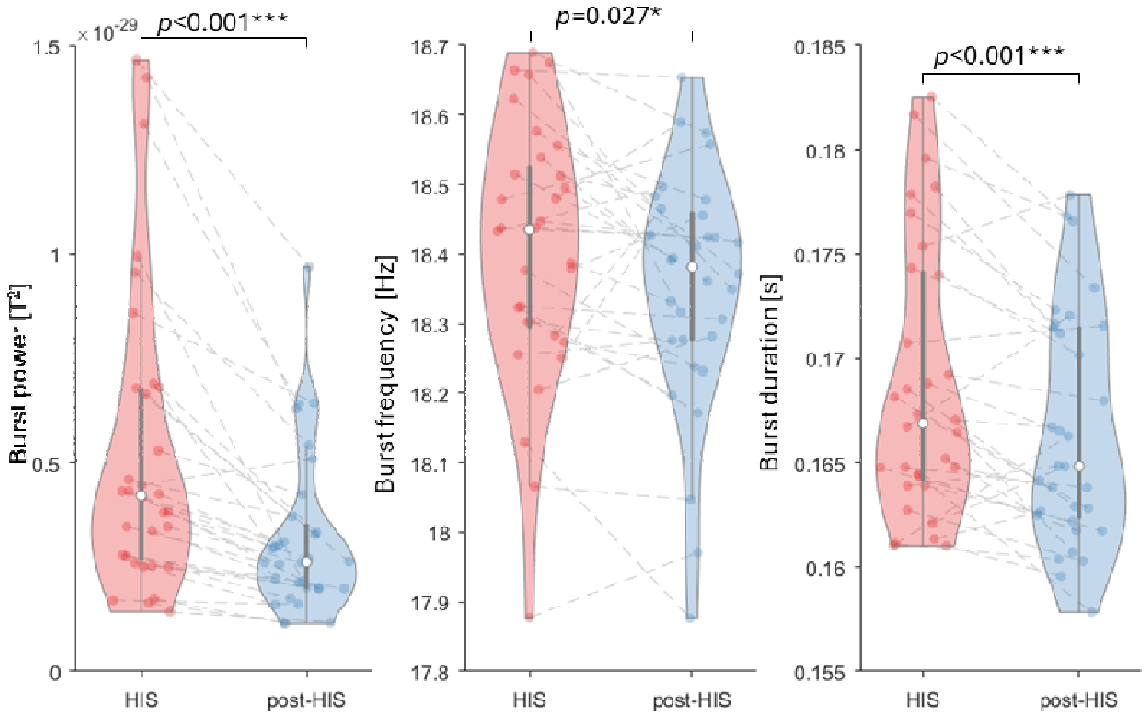

Figure S7: β band burst activity during HIS segments exhibited higher power, higher frequency, and longer duration than during post-HIS segments (paired t-tests). HIS segments were determined in each practice trial and each participant.

Supplementary Tables

Table S1: Our analysis identified four clustered brain regions contributing to θ/γ PAC difference during HIS segments relative to its time-shifted surrogates (n=200). Tables below document the subregions defined in HCP-MMP atlas contained within each cluster.

(A) Contralateral hippocampal cortex

Hemisphere ("L" or "R")	Area Name	Area Description	t_{31} value	*p* value
R	H	Hippocampus	2.76	3.76×10^{-3}
R	PHA1	ParaHippocampal area 1	3.58	5.77×10^{-4}
R	PHA2	ParaHippocampal area 2	3.98	1.91×10^{-4}
R	PHA3	ParaHippocampal area 3	4.07	1.52×10^{-4}

(B) Contralateral insula and orbitofrontal cortex

Hemisphere ("L" or "R")	Area Name	Area Description	t_{31} value	*p* value
R	13l	Area 13l	3.27	1.30×10^{-3}
R	OFC	Orbitofrontal cortex	3.92	2.29×10^{-4}
R	Pir	Piriform cortex	2.79	4.46×10^{-3}
R	AVI	Anterior Ventral Insular Area	2.87	3.71×10^{-3}
R	AAIC	Anterior Agranular Insula Complex	3.39	9.56×10^{-4}
R	TGd	Area TG dorsal	3.39	9.58×10^{-4}

(C) Bilateral vmPFC

Hemisphere	Area Name	Area Description	t_{31} value	*p* value

(“L” or “R”)				
L	p32	Area p32 prime	2.88	3.58×10^{-3}
L	10r	Area 10r	3.17	1.69×10^{-3}
R	10r	Area 10r	3.30	1.22×10^{-3}

(D) Ipsilateral parieto-occipital regions

Hemisphere (“L” or “R”)	Area Name	Area Description	t_{31} value	*p* value
L	V3A	Area V3A	3.49	7.30×10^{-4}
L	POS2	Parieto-Occipital Sulcus Area 2	2.88	3.53×10^{-3}
L	IPS1	IntraParietal Sulcus Area 1	3.03	2.45×10^{-3}
L	DVT	Dorsal Transitional Visual Area	2.93	3.12×10^{-3}
L	V6A	Area V6A	2.91	3.31×10^{-3}

Table S2: Our analysis identified three clustered brain regions contributing to β burst rate difference between HIS and post-HIS segments. Tables below document the subregions defined in HCP-MMP atlas contained within each cluster.

(A) Contralateral insula, frontal and temporal cortex

Hemisphere ("L" or "R")	Area Name	Area Description	t_{31} value	*p* value
R	PEF	Premotor Eye Fields	3.25	1.39×10^{-3}
R	6v	Ventral Area 6	3.64	4.93×10^{-4}
R	8C	Area 8C	2.77	4.73×10^{-3}
R	44	Area 44	2.72	5.24×10^{-3}
R	45	Area 45	3.50	5.25×10^{-4}
R	47l	Area 47l	2.57	7.58×10^{-3}
R	6r	Rostral Area 6	2.94	3.04×10^{-3}
R	IFJa	Area IFJa	2.89	3.48×10^{-3}
R	IFJp	Area IFJp	2.94	3.11×10^{-3}
R	IFSp	Area IFSp	4.21	1.02×10^{-4}
R	IFSa	Area IFSa	3.59	5.63×10^{-4}
R	p9-46v	Area posterior 9-46v	2.85	3.86×10^{-3}
R	47s	Area 47s	2.55	7.98×10^{-3}
R	PoI2	Posterior Insula area 2	3.04	2.42×10^{-3}
R	TA2	Area TA2	3.52	6.78×10^{-4}
R	FOP4	Frontal Opercular Area 4	3.76	3.53×10^{-4}
R	MI	Middle Insular Area	3.04	2.36×10^{-3}
R	Pir	Piriform cortex	3.07	2.21×10^{-3}

R	AVI	Anterior Ventral Insular Area	2.58	7.51×10^{-3}
R	AAIC	Anterior Agranular Insula Complex	4.42	5.57×10^{-5}
R	FOP1	Frontal Opercular Area 1	3.53	6.65×10^{-4}
R	FOP3	Frontal Opercular Area 3	3.53	6.63×10^{-4}
R	STGa	Area STGa	5.81	1.07×10^{-6}
R	A5	Auditory 5 Complex	3.25	1.38×10^{-3}
R	STSda	Area STSd anterior	4.25	9.06×10^{-5}
R	TGd	Area TG dorsal	3.33	1.13×10^{-3}
R	TE2a	Area TE2 anterior	3,86	2.68×10^{-4}
R	PoI1	Area Posterior Insular 1	3.11	1.99×10^{-3}
R	FOP5	Frontal Opercular Area 5	3.51	7.00×10^{-4}
R	p47r	Area posterior 47r	3.76	3.55×10^{-4}
R	STSva	Area STSv anterior	2.92	3.18×10^{-3}
R	TE1m	Area TE1 Middle	2.54	8.13×10^{-3}
R	PI	Para-Insular Area	3.70	4.23×10^{-4}

(B) Bilateral anterior cingulate cortex

Hemisphere (“L” or “R”)	Area Name	Area Description	t_{31} value	*p* value
L	d32	Area dorsal 32	3.10	2.07×10^{-3}
L	8BM	Area 8BM	3.69	4.26×10^{-4}
R	a24pr	Anterior 24 prime	3.70	4.09×10^{-4}
R	p32pr	Area p32 prime	2.47	9.51×10^{-3}
R	d32	Area dorsal 32	3.59	5.60×10^{-4}

R	8BM	Area 8BM	2.80	4.41×10^{-3}
R	a32pr	Area anterior 32 prime	3.27	1.33×10^{-3}
R	p24	Area posterior 24	3.04	2.41×10^{-3}

(C) Ipsilateral insula, frontal and temporal cortex

Hemisphere ("L" or "R")	Area Name	Area Description	t_{31} value	*p* value
L	A1	Primary Auditory Cortex	4.37	6.47×10^{-5}
L	44	Area 44	2.59	7.17×10^{-3}
L	43	Area 43	2.71	5.41×10^{-3}
L	OP4	Area OP4/PV	3.44	8.41×10^{-4}
L	OP1	Area OP1/SII	2.95	3.01×10^{-3}
L	OP2-3	Area OP2-3/VS	3.90	2.41×10^{-4}
L	52	Area 52	4.41	5.72×10^{-5}
L	PoI2	Posterior Insular Area 2	4.04	1.66×10^{-4}
L	TA2	Area TA2	3.54	6.44×10^{-4}
L	FOP1	Frontal Opercular Area 1	3.43	8.50×10^{-4}
L	FOP2	Frontal Opercular Area 2	3.14	1.86×10^{-3}
L	STGa	Area STGa	4.42	5.57×10^{-5}
L	PBelt	ParaBelt Complex	2.51	8.65×10^{-3}
L	A5	Auditory 5 Complex	3.40	9.36×10^{-4}
L	STSda	Area STSd anterior	4.83	1.73×10^{-5}
L	TE1a	Area TE1 anterior	2.57	7.62×10^{-3}
L	PFop	Area PF opercular	4.29	8.06×10^{-5}

L	PoI1	Area Posterior Insular 1	3.12	1.96×10^{-3}
L	Ig	Insular Granular Complex	3.24	1.41×10^{-3}
L	MBelt	Medial Belt Complex	4.04	1.64×10^{-4}
L	A4	Auditory 4 Complex	3.00	2.65×10^{-3}
L	STSva	Area STSv anterior	4.15	1.19×10^{-4}
L	TE1m	Area TE1 Middle	2.51	8.66×10^{-3}
L	PI	Para-Insular Area	2.46	9.75×10^{-3}

During the preparation of this work the author(s) used GPT 4.0 for text editing purposes. After using this tool/service, the author(s) reviewed and edited the content as needed and take(s) full responsibility for the content of the published article.

References

1. Bönstrup, M., Iturrate, I., Thompson, R., Cruciani, G., Censor, N., and Cohen, L.G. (2019). A Rapid Form of Offline Consolidation in Skill Learning. Curr Biol *29*, 1346-1351 e1344. 10.1016/j.cub.2019.02.049.
2. Doyon, J., and Benali, H. (2005). Reorganization and plasticity in the adult brain during learning of motor skills. Current opinion in neurobiology *15*, 161-167. 10.1016/j.conb.2005.03.004.
3. Dehaene, S., Meyniel, F., Wacongne, C., Wang, L., and Pallier, C. (2015). The Neural Representation of Sequences: From Transition Probabilities to Algebraic Patterns and Linguistic Trees. Neuron *88*, 2-19. 10.1016/j.neuron.2015.09.019.
4. Dayan, E., and Cohen, L.G. (2011). Neuroplasticity subserving motor skill learning. Neuron *72*, 443-454. 10.1016/j.neuron.2011.10.008.
5. Albouy, G., King, B.R., Maquet, P., and Doyon, J. (2013). Hippocampus and striatum: dynamics and interaction during acquisition and sleep-related motor sequence memory consolidation. Hippocampus *23*, 985-1004. 10.1002/hipo.22183.
6. Breton, J., and Robertson, E.M. (2014). Flipping the switch: mechanisms that regulate memory consolidation. Trends Cogn Sci *18*, 629-634. 10.1016/j.tics.2014.08.005.
7. Buch, E.R., Claudino, L., Quentin, R., Bönstrup, M., and Cohen, L.G. (2021). Consolidation of human skill linked to waking hippocampo-neocortical replay. Cell Rep *35*, 109193. 10.1016/j.celrep.2021.109193.
8. Jacobacci, F., Armony, J.L., Yeffal, A., Lerner, G., Amaro, E., Jr., Jovicich, J., Doyon, J., and Della-Maggiore, V. (2020). Rapid hippocampal plasticity supports motor sequence learning. Proc Natl Acad Sci U S A *117*, 23898-23903. 10.1073/pnas.2009576117.
9. Mylonas, D., Schapiro, A.C., Verfaellie, M., Baxter, B., Vangel, M., Stickgold, R., and Manoach, D.S. (2024). Maintenance of Procedural Motor Memory across Brief Rest Periods Requires the Hippocampus. J Neurosci *44*. 10.1523/JNEUROSCI.1839-23.2024.
10. Hayward, W., Buch, E.R., Norato, G., Iwane, F., Dash, D., Salamanca-Giron, R.F., Bartrum, E., Walitt, B., Nath, A., and Cohen, L.G. (2024). Procedural Motor Memory Deficits in Patients With Long-COVID. Neurology *102*, e208073. 10.1212/WNL.0000000000208073.

11. Brooks, E., Wallis, S., Hendrikse, J., and Coxon, J. (2024). Micro-consolidation occurs when learning an implicit motor sequence, but is not influenced by HIIT exercise. NPJ Sci Learn *9*, 23. 10.1038/s41539-024-00238-6.

12. Bönstrup, M., Iturrate, I., Hebart, M.N., Censor, N., and Cohen, L.G. (2020). Mechanisms of offline motor learning at a microscale of seconds in large-scale crowdsourced data. NPJ Sci Learn *5*, 7. 10.1038/s41539-020-0066-9.

13. Chen, P.-C., Stritzelberger, J., Walther, K., Hamer, H., and Staresina, B.P. (2024). Hippocampal ripples during offline periods predict human motor sequence learning. bioRxiv, 2024.2010.2006.614680. 10.1101/2024.10.06.614680.

14. Sjøgård, M., Baxter, B., Mylonas, D., Driscoll, B., Kwok, K., Tolosa, A., Thompson, M., Stickgold, R., Vangel, M., Chu, C., and Manoach, D.S. (2024). Hippocampal ripples mediate motor learning during brief rest breaks in humans. bioRxiv. https://doi.org/10.1101/2024.05.02.592200.

15. Griffin, S., Khanna, P., Choi, H., Thiesen, K., Novik, L., Morecraft, R.J., and Ganguly, K. (2025). Ensemble reactivations during brief rest drive fast learning of sequences. Nature. 10.1038/s41586-024-08414-9.

16. Dash, D., Iwane, F., Hayward, W., Salamanca-Giron, R.F., Bonstrup, M., Buch, E.R., and Cohen, L.G. (2025). Sequence action representations contextualize during early skill learning. Elife *13*. 10.7554/eLife.102475.

17. Nassar, M.R., Helmers, J.C., and Frank, M.J. (2018). Chunking as a rational strategy for lossy data compression in visual working memory. Psychol Rev *125*, 486-511. 10.1037/rev0000101.

18. Lashley, K.S. (1951). The problem of serial order in behavior. In Cerebral mechanisms in behavior: The Hixon Symposium, L.A. Jeffress, ed. (Wiley), pp. 112-146.

19. Gobet, F., and Clarkson, G. (2004). Chunks in expert memory: evidence for the magical number four … or is it two? Memory *12*, 732-747. 10.1080/09658210344000530.

20. Baddeley, A. (2003). Working memory: looking back and looking forward. Nat Rev Neurosci *4*, 829-839. 10.1038/nrn1201.

21. Cowan, N. (2008). What are the differences between long-term, short-term, and working memory? Prog Brain Res *169*, 323-338. 10.1016/S0079-6123(07)00020-9.

22. Constantinidis, C., and Klingberg, T. (2016). The neuroscience of working memory capacity and training. Nat Rev Neurosci *17*, 438-449. 10.1038/nrn.2016.43.

23. Sakai, K., Kitaguchi, K., and Hikosaka, O. (2003). Chunking during human visuomotor sequence learning. Exp Brain Res *152*, 229-242. 10.1007/s00221-003-1548-8.

24. Branscheidt, M., Kassavetis, P., Anaya, M., Rogers, D., Huang, H.D., Lindquist, M.A., and Celnik, P. (2019). Fatigue induces long-lasting detrimental changes in motor-skill learning. Elife *8*. 10.7554/eLife.40578.

25. Sharples, S.A., Gould, J.A., Vandenberk, M.S., and Kalmar, J.M. (2016). Cortical Mechanisms of Central Fatigue and Sense of Effort. PLoS One *11*, e0149026. 10.1371/journal.pone.0149026.

26. Daume, J., Kaminski, J., Schjetnan, A.G.P., Salimpour, Y., Khan, U., Kyzar, M., Reed, C.M., Anderson, W.S., Valiante, T.A., Mamelak, A.N., and Rutishauser, U. (2024). Control of working memory by phase-amplitude coupling of human hippocampal neurons. Nature *629*, 393-401. 10.1038/s41586-024-07309-z.

27. Foster, D.J., and Wilson, M.A. (2007). Hippocampal theta sequences. Hippocampus *17*, 1093-1099. 10.1002/hipo.20345.

28. Skaggs, W.E., McNaughton, B.L., Wilson, M.A., and Barnes, C.A. (1996). Theta phase precession in hippocampal neuronal populations and the compression of temporal sequences. Hippocampus *6*, 149-172. 10.1002/(SICI)1098-1063(1996)6:2<149::AID-HIPO6>3.0.CO;2-K.

29. Zheng, J., Yebra, M., Schjetnan, A.G.P., Patel, K., Katz, C.N., Kyzar, M., Mosher, C.P., Kalia, S.K., Chung, J.M., Reed, C.M., et al. (2024). Theta phase precession supports memory formation and retrieval of naturalistic experience in humans. Nat Hum Behav *8*, 2423-2436. 10.1038/s41562-024-01983-9.

30. Kaminski, J., Brzezicka, A., and Wrobel, A. (2011). Short-term memory capacity (7 +/- 2) predicted by theta to gamma cycle length ratio. Neurobiol Learn Mem *95*, 19-23. 10.1016/j.nlm.2010.10.001.

31. Lisman, J.E., and Jensen, O. (2013). The theta-gamma neural code. Neuron *77*, 1002-1016. 10.1016/j.neuron.2013.03.007.

32. Lizarazu, M., Carreiras, M., and Molinaro, N. (2023). Theta-gamma phase-amplitude coupling in auditory cortex is modulated by language proficiency. Hum Brain Mapp *44*, 2862-2872. 10.1002/hbm.26250.

33. Akkad, H., Dupont-Hadwen, J., Kane, E., Evans, C., Barrett, L., Frese, A., Tetkovic, I., Bestmann, S., and Stagg, C.J. (2021). Increasing human motor skill acquisition by driving theta-gamma coupling. Elife *10*. 10.7554/eLife.67355.

34. Griffiths, B.J., Mayhew, S.D., Mullinger, K.J., Jorge, J., Charest, I., Wimber, M., and Hanslmayr, S. (2019). Alpha/beta power decreases track the fidelity of stimulus-specific information. Elife *8*. 10.7554/eLife.49562.

35. Hanslmayr, S., Staudigl, T., and Fellner, M.C. (2012). Oscillatory power decreases and long-term memory: the information via desynchronization hypothesis. Front Hum Neurosci *6*, 74. 10.3389/fnhum.2012.00074.

36. Griffiths, B.J., Martin-Buro, M.C., Staresina, B.P., and Hanslmayr, S. (2021). Disentangling neocortical alpha/beta and hippocampal theta/gamma oscillations in human episodic memory formation. Neuroimage *242*, 118454. 10.1016/j.neuroimage.2021.118454.

37. Kavanaugh, B.C., Vigne, M.M., Thorpe, R., Legere, C., Acuff, W.L., Vaughan, N., Tirrell, E., Haegens, S., Carpenter, L.L., and Jones, S.R. (2023). The association between oscillatory burst features and deviations during human working memory. BioxRiv *https://doi.org/10.1101/2024.12.06.622989*.

38. Lundqvist, M., Rose, J., Herman, P., Brincat, S.L., Buschman, T.J., and Miller, E.K. (2016). Gamma and Beta Bursts Underlie Working Memory. Neuron *90*, 152-164. 10.1016/j.neuron.2016.02.028.

39. Lundqvist, M., Miller, E.K., Nordmark, J., Liljefors, J., and Herman, P. (2024). Beta: bursts of cognition. Trends Cogn Sci *28*, 662-676. 10.1016/j.tics.2024.03.010.

40. Enoka, R.M., and Duchateau, J. (2008). Muscle fatigue: what, why and how it influences muscle function. J Physiol *586*, 11-23. 10.1113/jphysiol.2007.139477.

41. Ariani, G., and Diedrichsen, J. (2019). Sequence learning is driven by improvements in motor planning. J Neurophysiol *121*, 2088-2100. 10.1152/jn.00041.2019.

42. Blischke, K., and Malangre, A. (2016). Chunk concatenation evolves with practice and sleep-related enhancement consolidation in a complex arm movement sequence. J Hum Kinet *51*, 5-17. 10.1515/hukin-2015-0163.

43. Heusser, A.C., Poeppel, D., Ezzyat, Y., and Davachi, L. (2016). Episodic sequence memory is supported by a theta-gamma phase code. Nat Neurosci *19*, 1374-1380. 10.1038/nn.4374.

44. Abubaker, M., Al Qasem, W., Pilatova, K., Jezdik, P., and Kvasnak, E. (2024). Theta-gamma-coupling as predictor of working memory performance in young and elderly healthy people. Mol Brain *17*, 74. 10.1186/s13041-024-01149-8.

45. Pan, S.C., and Rickard, T.C. (2015). Sleep and motor learning: Is there room for consolidation? Psychol Bull *141*, 812-834. 10.1037/bul0000009.

46. Enoka, R.M., and Duchateau, J. (2016). Translating Fatigue to Human Performance. Med Sci Sports Exerc *48*, 2228-2238. 10.1249/MSS.0000000000000929.

47. Nieuwenhuis, S., Ridderinkhof, K.R., de Jong, R., Kok, A., and van der Molen, M.W. (2000). Inhibitory inefficiency and failures of intention activation: age-related decline in the control of saccadic eye movements. Psychol Aging *15*, 635-647.

48. Sweller, J. (2018). Measuring cognitive load. Perspect Med Educ *7*, 1-2. 10.1007/s40037-017-0395-4.

49. Wickens, C.D., Hutchins, S., Carolan, T., and Cumming, J. (2013). Effectiveness of part-task training and increasing-difficulty training strategies: a meta-analysis approach. Hum Factors *55*, 461-470. 10.1177/0018720812451994.

50. Miller, G.A. (1956). The magical number seven plus or minus two: some limits on our capacity for processing information. Psychol Rev *63*, 81-97.

51. Verwey, W.B., and Eikelboom, T. (2003). Evidence for lasting sequence segmentation in the discrete sequence-production task. J Mot Behav *35*, 171-181. 10.1080/00222890309602131.

52. Kennerley, S.W., Sakai, K., and Rushworth, M.F. (2004). Organization of action sequences and the role of the pre-SMA. J Neurophysiol *91*, 978-993. 10.1152/jn.00651.2003

00651.2003 [pii].

53. Verwey, W.B., and Dronkert, Y. (1996). Practicing a Structured Continuous Key-Pressing Task: Motor Chunking or Rhythm Consolidation? J Mot Behav *28*, 71-79. 10.1080/00222895.1996.9941735.

54. Hikosaka, O., Nakahara, H., Rand, M.K., Sakai, K., Lu, X., Nakamura, K., Miyachi, S., and Doya, K. (1999). Parallel neural networks for learning sequential procedures. Trends Neurosci *22*, 464-471.

55. Shea, C.H., Park, J.H., and Braden, H.W. (2006). Age-related effects in sequential motor learning. Phys Ther *86*, 478-488.

56. Abrahamse, E.L., Jimenez, L., Verwey, W.B., and Clegg, B.A. (2010). Representing serial action and perception. Psychon Bull Rev *17*, 603-623. 10.3758/PBR.17.5.603.

57. Seidler, R.D., Bo, J., and Anguera, J.A. (2012). Neurocognitive contributions to motor skill learning: the role of working memory. J Mot Behav *44*, 445-453. 10.1080/00222895.2012.672348.

58. Allen, J.G., Scovern, A.W., Logue, A.M., and Coyne, L. (1988). Indications for extended psychiatric hospitalization: a study of clinical opinion. Compr Psychiatry *29*, 604-612. 10.1016/0010-440x(88)90081-8.

59. McDougle, S.D., and Hillman, H. (2025). Motor working memory. Trends Cogn Sci. 10.1016/j.tics.2025.08.011.

60. Griffiths, B.J., Parish, G., Roux, F., Michelmann, S., van der Plas, M., Kolibius, L.D., Chelvarajah, R., Rollings, D.T., Sawlani, V., Hamer, H., et al. (2019). Directional coupling of slow and fast hippocampal gamma with neocortical alpha/beta oscillations in human episodic memory. Proc Natl Acad Sci U S A *116*, 21834-21842. 10.1073/pnas.1914180116.

61. Parish, G., Hanslmayr, S., and Bowman, H. (2018). The Sync/deSync Model: How a Synchronized Hippocampus and a Desynchronized Neocortex Code Memories. J Neurosci *38*, 3428-3440. 10.1523/JNEUROSCI.2561-17.2018.

62. Hanslmayr, S., Staresina, B.P., and Bowman, H. (2016). Oscillations and Episodic Memory: Addressing the Synchronization/Desynchronization Conundrum. Trends Neurosci *39*, 16-25. 10.1016/j.tins.2015.11.004.

63. Griffiths, B.J., and Fuentemilla, L. (2020). Event conjunction: How the hippocampus integrates episodic memories across event boundaries. Hippocampus *30*, 162-171. 10.1002/hipo.23161.

64. Herman, P.A., Lundqvist, M., and Lansner, A. (2013). Nested theta to gamma oscillations and precise spatiotemporal firing during memory retrieval in a simulated attractor network. Brain Res *1536*, 68-87. 10.1016/j.brainres.2013.08.002.

65. Lundqvist, M., Herman, P., and Lansner, A. (2011). Theta and gamma power increases and alpha/beta power decreases with memory load in an attractor network model. J Cogn Neurosci *23*, 3008-3020. 10.1162/jocn_a_00029.

66. Mi, Y., Katkov, M., and Tsodyks, M. (2017). Synaptic Correlates of Working Memory Capacity. Neuron *93*, 323-330. 10.1016/j.neuron.2016.12.004.

67. Lisman, J.E., and Idiart, M.A. (1995). Storage of 7 +/- 2 short-term memories in oscillatory subcycles. Science *267*, 1512-1515. 10.1126/science.7878473.

68. Jensen, O., and Lisman, J.E. (2005). Hippocampal sequence-encoding driven by a cortical multi-item working memory buffer. Trends Neurosci *28*, 67-72. 10.1016/j.tins.2004.12.001.

69. Colgin, L.L. (2015). Theta-gamma coupling in the entorhinal-hippocampal system. Curr Opin Neurobiol *31*, 45-50. 10.1016/j.conb.2014.08.001.

70. Gillespie, A.K., Astudillo Maya, D.A., Denovellis, E.L., Liu, D.F., Kastner, D.B., Coulter, M.E., Roumis, D.K., Eden, U.T., and Frank, L.M. (2021). Hippocampal replay reflects specific past experiences rather than a plan for subsequent choice. Neuron. 10.1016/j.neuron.2021.07.029.

71. Kavanaugh, B.C., Vigne, M.M., Gamble, I., Legere, C., DePamphilis, G., Acuff, W.L., Tirrell, E., Vaughan, N., Thorpe, R., Spirito, A., et al. (2024). Dysfunctional oscillatory bursting patterns underlie working memory deficits in adolescents with ADHD. bioRxiv. 10.1101/2024.12.09.627520.

72. Liljefors, J., Almeida, R., Rane, G., Lundstrom, J.N., Herman, P., and Lundqvist, M. (2024). Distinct functions for beta and alpha bursts in gating of human working memory. Nat Commun *15*, 8950. 10.1038/s41467-024-53257-7.

73. Lundqvist, M., Herman, P., Warden, M.R., Brincat, S.L., and Miller, E.K. (2018). Gamma and beta bursts during working memory readout suggest roles in its volitional control. Nat Commun *9*, 394. 10.1038/s41467-017-02791-8.

74. Eysenck, H.J. (1965). A Three-Factor Theory of Reminiscence. Br J Psychol *56*, 163-182. 10.1111/j.2044-8295.1965.tb00956.x.

75. Torok, B., Janacsek, K., Nagy, D.G., Orban, G., and Nemeth, D. (2017). Measuring and filtering reactive inhibition is essential for assessing serial decision making and learning. J Exp Psychol Gen *146*, 529-542. 10.1037/xge0000288.

76. Ariani, G., Kwon, Y.H., and Diedrichsen, J. (2020). Repetita iuvant: repetition facilitates online planning of sequential movements. J Neurophysiol *123*, 1727-1738. 10.1152/jn.00054.2020.

77. Karni, A., Meyer, G., Jezzard, P., Adams, M.M., Turner, R., and Ungerleider, L.G. (1995). Functional MRI evidence for adult motor cortex plasticity during motor skill learning. Nature *377*, 155-158. 10.1038/377155a0.

78. Walker, M.P., and Stickgold, R. (2004). Sleep-dependent learning and memory consolidation. Neuron *44*, 121-133.

79. Iwane, F., Dash, D., Salamanca-Giron, R.F., Hayward, W., Bönstrup, M., Buch, E.R., and Cohen, L.G. (2023). Combined low-frequency brain oscillatory activity and behavior predict future errors in human motor skill. Curr Biol *33*, 3145-3154 e3145. 10.1016/j.cub.2023.06.040.

80. Oostenveld, R., Fries, P., Maris, E., and Schoffelen, J.-M. (2011). FieldTrip: open source software for advanced analysis of MEG, EEG, and invasive electrophysiological data. Computational intelligence and neuroscience *2011*, 1-9.

81. Fischl, B. (2012). FreeSurfer. Neuroimage *62*, 774-781. 10.1016/j.neuroimage.2012.01.021.

82. Marcus, D.S., Harwell, J., Olsen, T., Hodge, M., Glasser, M.F., Prior, F., Jenkinson, M., Laumann, T., Curtiss, S.W., and Van Essen, D.C. (2011). Informatics and data mining tools and strategies for the human connectome project. Front Neuroinform *5*, 4. 10.3389/fninf.2011.00004.

83. Delorme, A., and Makeig, S. (2004). EEGLAB: an open source toolbox for analysis of single-trial EEG dynamics including independent component analysis. Journal of neuroscience methods *134*, 9-21.

84. Tort, A.B., Komorowski, R., Eichenbaum, H., and Kopell, N. (2010). Measuring phase-amplitude coupling between neuronal oscillations of different frequencies. J Neurophysiol *104*, 1195-1210. 10.1152/jn.00106.2010.

85. Vaz, A.P., Yaffe, R.B., Wittig, J.H., Jr., Inati, S.K., and Zaghloul, K.A. (2017). Dual origins of measured phase-amplitude coupling reveal distinct neural mechanisms underlying episodic memory in the human cortex. Neuroimage *148*, 148-159. 10.1016/j.neuroimage.2017.01.001.

86. Norman, Y., Yeagle, E.M., Khuvis, S., Harel, M., Mehta, A.D., and Malach, R. (2019). Hippocampal sharp-wave ripples linked to visual episodic recollection in humans. Science *365*. 10.1126/science.aax1030.

87. Aru, J., Aru, J., Priesemann, V., Wibral, M., Lana, L., Pipa, G., Singer, W., and Vicente, R. (2015). Untangling cross-frequency coupling in neuroscience. Curr Opin Neurobiol *31*, 51-61. 10.1016/j.conb.2014.08.002.

88. Shin, H., Law, R., Tsutsui, S., Moore, C.I., and Jones, S.R. (2017). The rate of transient beta frequency events predicts behavior across tasks and species. Elife *6*. 10.7554/eLife.29086.

89. Maris, E., and Oostenveld, R. (2007). Nonparametric statistical testing of EEG- and MEG-data. J Neurosci Methods *164*, 177-190. 10.1016/j.jneumeth.2007.03.024.